iScience

CellPress
OPEN ACCESS

Article

The Rho1 GTPase controls anillo-septin assembly to facilitate contractile ring closure during cytokinesis

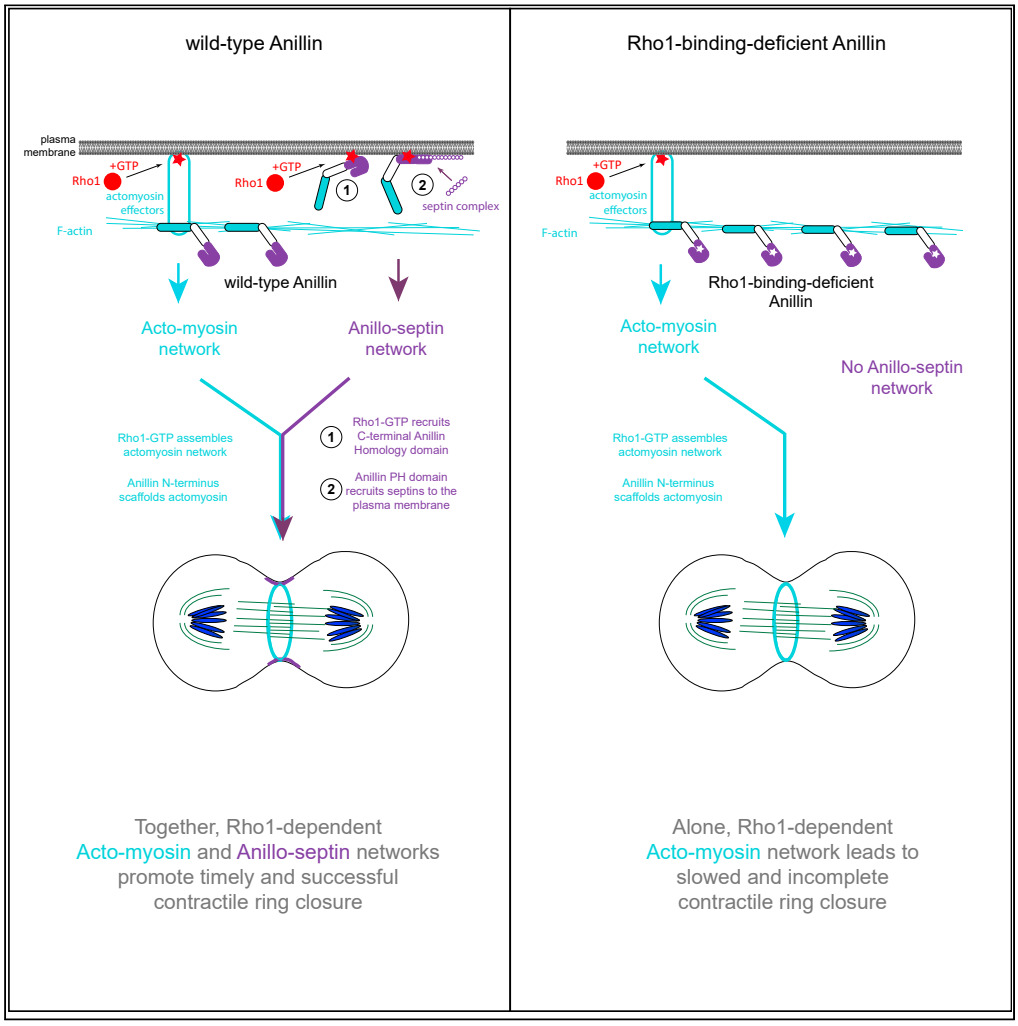

Sabrya C. Carim, Gilles R.X. Hickson

gilles.hickson@umontreal.ca

Highlights

Anillin recruits septins to the contractile ring independently of actomyosin

Rho1-GTP binding to the Anillin C-terminus is a prerequisite to septin recruitment

Rho1-dependent anillo-septin assembly facilitates contractile ring closure

Rho1-dependent anillo-septin assembly is conserved from flies to humans

Carim & Hickson, iScience 26, 106903
June 16, 2023
https://doi.org/10.1016/j.isci.2023.106903

iScience

CellPress
OPEN ACCESS

Article

The Rho1 GTPase controls anillo-septin assembly to facilitate contractile ring closure during cytokinesis

Sabrya C. Carim[1] and Gilles R.X. Hickson[1,2,3,*]

SUMMARY

Animal cell cytokinesis requires activation of the GTPase RhoA (Rho1 in *Drosophila*), which assembles an F-actin- and myosin II-dependent contractile ring (CR) at the equatorial plasma membrane. CR closure is poorly understood, but involves the multidomain scaffold protein, Anillin. Anillin binds many CR components including F-actin and myosin II (collectively actomyosin), RhoA and the septins. Anillin recruits septins to the CR but the mechanism is unclear. Live imaging of *Drosophila* S2 cells and HeLa cells revealed that the Anillin N-terminus, which scaffolds actomyosin, cannot recruit septins to the CR. Rather, septin recruitment required the ability of the Anillin C-terminus to bind Rho1-GTP and the presence of the Anillin PH domain, in a sequential mechanism occurring at the plasma membrane, independently of F-actin. Anillin mutations that blocked septin recruitment, but not actomyosin scaffolding, slowed CR closure and disrupted cytokinesis. Thus, CR closure requires coordination of two Rho1-dependent networks: actomyosin and anillo-septin.

INTRODUCTION

Cytokinesis of animal cells involves dramatic remodeling of the equatorial plasma membrane via the formation of a dynamic cleavage furrow. The cleavage furrow contains F-actin and non-muscle myosin II, collectively referred to as actomyosin. Furrow ingression is driven by a contractile ring (CR) that forms and constricts at the midpoint, or apex, of the cleavage furrow. Both furrow assembly and CR constriction require the continuous spindle-directed activation of the RhoA GTPase (Rho1 in *Drosophila*).[1] Active GTP-bound RhoA generated at the equatorial plasma membrane recruits and activates formins, which polymerize unbranched F-actin, and Rho-kinase, which activates myosin II.[2–5] Thus active RhoA assembles an actomyosin-based, membrane-anchored network that generates tension during furrow assembly and CR constriction.[6] The pioneering work of Schroeder 50 years ago revealed that CRs disassemble as they constrict,[7] but the mechanisms controlling CR closure and disassembly are still not understood.[8]

The scaffold protein, Anillin, is a key regulator of CRs that is required for their complete and stable closure.[9–12] Through conserved domains in its N-terminus, Anillin can bind both F-actin and myosin II.[11,13,14] Anillin's ability to cross-link actin filaments[13,14] can generate pN forces independently of myosin motors *in vitro*,[15] an activity that likely promotes CR closure *in vivo*. The Anillin N-terminus can also bind a host of other proteins.[16,17] These include the Citron kinase (Sticky in *Drosophila*),[18,19] another RhoA-GTP target,[20] with which Anillin cooperates to form the stable midbody ring that persists after CR closure.[18] In addition, the Anillin C-terminus can bind to RhoA-GTP, membrane lipids and septins,[10,21–23] and importins.[24] As such, Anillin can be considered a master organizer of the CR and the subsequent midbody ring, although how it coordinates different cytoskeletal elements to remodel the plasma membrane remains unresolved.

Septins are conserved cytoskeletal proteins and components of cleavage furrows of organisms as diverse as yeast and humans.[25,26] Septins form palindromic, oligomeric complexes: tetramers in worms, hexamers in flies and mammals and octamers in mammals and yeast. Septin complexes assemble into membrane-associated filaments that can serve as membrane-diffusion barriers.[27] Septins can form higher order structures such as rings and gauzes.[25] In *Drosophila*, the canonical hexamer comprises Sep1, Sep2, and Peanut (Pnut),[28] orthologs of mammalian SEPT2, SEPT6 and SEPT7, respectively. According to the recent reordering of septin complexes,[29–31] hexamers are arranged as follows: Sep1-Sep2-Pnut-Pnut-Sep2-Sep1. The

[1]CHU Sainte-Justine Research Center, 3175 Chemin de la Côte Ste-Catherine, Montréal, QC H3T 1C5, Canada

[2]Département de Pathologie et Biologie Cellulaire, Faculté de Médecine, Université de Montréal, P.O. Box 6128, Station Centre-Ville, Montréal, QC H3C 3J7, Canada

[3]Lead contact

*Correspondence: gilles.hickson@umontreal.ca

https://doi.org/10.1016/j.isci.2023.106903

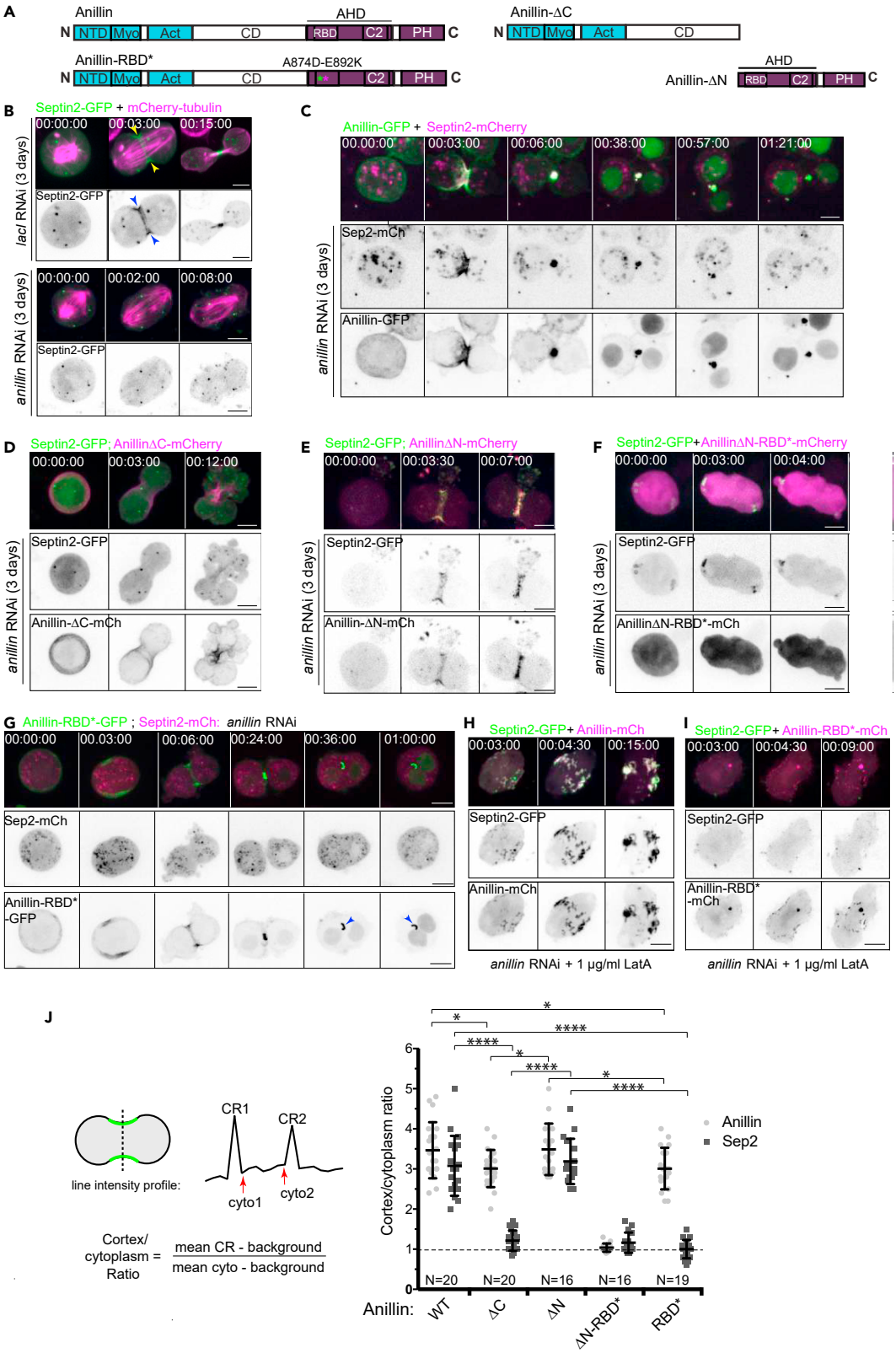
A
Anillin
AHD
N NTD Myo Act CD RBD C2 PH C
Anillin-ΔC
N NTD Myo Act CD
Anillin-RBD*
A874D-E892K
N NTD Myo Act CD * C2 PH C
Anillin-ΔN
AHD
RBD C2 PH C
B
Septin2-GFP + mCherry-tubulin
lacI RNAi (3 days)
00:00:00 00:03:00 00:15:00
Septin2-GFP
anillin RNAi (3 days)
00:00:00 00:02:00 00:08:00
Septin2-GFP
C
Anillin-GFP + Septin2-mCherry
00:00:00 00:03:00 00:06:00 00:38:00 00:57:00 01:21:00
anillin RNAi (3 days)
Sep2-mCh
Anillin-GFP
D
Septin2-GFP; AnillinΔC-mCherry
00:00:00 00:03:00 00:12:00
anillin RNAi (3 days)
Septin2-GFP
Anillin-ΔC-mCh
E
Septin2-GFP; AnillinΔN-mCherry
00:00:00 00:03:30 00:07:00
anillin RNAi (3 days)
Septin2-GFP
Anillin-ΔN-mCh
F
Septin2-GFP+AnillinΔN-RBD*-mCherry
00:00:00 00:03:00 00:04:00
anillin RNAi (3 days)
Septin2-GFP
AnillinΔN-RBD*-mCh
G
Anillin-RBD*-GFP ; Septin2-mCh: anillin RNAi
00:00:00 00:03:00 00:06:00 00:24:00 00:36:00 01:00:00
Sep2-mCh
Anillin-RBD*-GFP
H
Septin2-GFP+ Anillin-mCh
00:03:00 00:04:30 00:15:00
Septin2-GFP
Anillin-mCh
anillin RNAi + 1 µg/ml LatA
I
Septin2-GFP+ Anillin-RBD*-mCh
00:03:00 00:04:30 00:09:00
Septin2-GFP
Anillin-RBD*-mCh
anillin RNAi + 1 µg/ml LatA
J
CR1
CR2
line intensity profile:
cyto1
cyto2
Cortex/cytoplasm Ratio = mean CR - background / mean cyto - background
Cortex/cytoplasm ratio
Anillin
Sep2
N=20 N=20 N=16 N=16 N=19
Anillin: WT ΔC ΔN ΔN-RBD* RBD*

Figure 1. The recruitment of Septin2 to the cleavage furrow requires the Rho1-GTP binding-competent Anillin-C-terminus

(A) Cartoon representations of *Drosophila* Anillin, wild-type and mutant constructs. Domains are labeled follows: N-terminal domain (NTD); myosin binding domain (Myo); F-actin binding domain (Act); central domain (CD); Anillin homology domain (AHD), comprising a Rho1-GTP binding domain (RBD) and a C2 domain; and a Pleckstrin homology (PH) domain. Asterisks denote the positions of the A874D and E892K mutations shown to abrogate RhoA-GTP binding to the human ANLN RBD.[23]

(B–I) Representative, high-resolution time-lapse sequences of transiently transfected S2 cells inducibly expressing Septin2-GFP (B, D–F, and H-I; green in merged panels) or Septin2-mCherry (C, G; magenta in merged panels) following LacI control RNAi (B, upper panels) or endogenous Anillin RNAi (B, lower panels and C-I) for three days. Cells were co-expressing mCherry-tubulin (B-C) or different RNAi-resistant mCherry-tagged Anillin constructs as indicated. Cells in H and I were pre-treated with LatA 30–60 min before imaging.

(J) Quantification of enrichment of Septin2-GFP and Anillin-mCherry at mid-cleavage equatorial cortices in cells expressing the indicated Anillin constructs following endogenous Anillin RNAi. Normalized cortex/cytoplasmic intensity ratios for both the indicated mCherry-tagged Anillin constructs and Sep2-GFP obtained from line profile measurements are shown for N = 16–20 cells per condition, from 3 independent experiments. Bars represent mean values and SD. Statistical analysis is by two-way ANOVA with Sidak's multiple comparisons test: *p<0.05, ****, p<0.0001 (For clarity, p values are not shown for the ΔN-RBD* condition). Times are h:min:s and scale bars are 5 μm. See also Figure S1.

roles and organization of septins at animal cell cleavage furrows are unknown, although they promote the normal asymmetric closure of the CR.[32] In worm, fly and human cells, septins are recruited to cleavage furrows by Anillin.[9,21,22,33] However, Anillin-dependent septin recruitment could involve both direct and indirect mechanisms. First, septins can bind the C-terminal Pleckstrin homology (PH) domain of Anillin.[21,22,34,35] Second, septins can also bind F-actin[36] and myosin II,[37] both of which are key CR components that Anillin scaffolds[11,13,14] (see Figure 1A for Anillin domain organization). Thus, it remains unclear to what extent actomyosin-dependent interactions contribute to Anillin-dependent septin localization during cytokinesis. We sought to determine how Anillin recruits septins to the CR and to test the functional consequences of this recruitment during CR closure.

RESULTS

The recruitment of septins to the cleavage furrow depends on the Rho1-GTP binding-competent anillin-C-terminus

We wished to examine septin localization in live, actively dividing *Drosophila* S2 cells. These cells express Sep1, Sep2 and Peanut (Pnut), which form the canonical septin hexamer.[28] Expression of Pnut-GFP induced the formation of aberrant cytoplasmic structures and was therefore not examined further (not shown). However, Sep1-GFP and Sep2-GFP mimicked the endogenous Pnut localization that we previously described,[9] which includes robust recruitment to the CR (Figures 1B and S1A) and localization to cytoplasmic rings and tubes (not shown). As expected, the localization of Sep1-GFP and Sep2-GFP to the cleavage furrow was abolished on RNAi-mediated depletion of Anillin (Figures 1B and S1A). Similarly, Anillin depletion abrogated the furrow localization of endogenous Pnut, as evidenced in fixed untransfected cells stained with a Pnut-specific antibody (Figure S1B), and as we previously reported.[9] Thus, the furrow recruitment of Sep1, Sep2 and Pnut is wholly dependent on Anillin. We next performed rescue experiments using mutant versions of RNAi resistant Anillin (see Figures S1C and S1D). Co-expression of wild-type, RNAi-resistant Anillin-mCherry rescued the recruitment of both Sep2-GFP (Figure 1C, quantified in Figure 1J) and Sep1-GFP (Figure S1E) to the CR following endogenous Anillin depletion. Because septins exist only in hexameric complexes that depend on Sep1, Sep2, and Pnut for stability,[28] we proceeded to use Sep2-GFP as a marker for the entire septin complex. Expression of Anillin-ΔC, which lacks the C-terminal Anillin homology (AH) and PH domains, failed to restore Sep2-GFP recruitment to the CR (Figure 1D, quantified in Figure 1J). This construct (Anillin-ΔC) was previously shown to retain the ability to scaffold actomyosin and to allow the formation of partially functional CRs and stable midbody ring-like structures.[38] In stark contrast, expression of the C-terminal AH-PH region (i.e., Anillin-ΔN), was sufficient to robustly recruit Sep2-GFP to the equatorial plasma membrane at the onset of cytokinesis (Figure 1E and Video S1, quantified in Figure 1J). We conclude that Sep2-containing hexamers are recruited to the CR uniquely via the C-terminus of Anillin, and not via the actomyosin sub-network, even when this is scaffolded by the Anillin N-terminus.

The C-terminal Anillin AH domain contains a Rho1-binding domain (RBD), whose crystal structure was solved for human ANLN bound to RhoA-GTP.[23] To test the potential involvement of Rho1 in regulating Anillin's ability to recruit septins to the cleavage furrow, we mutated residues within the *Drosophila* RBD (A874D and E892K) that are orthologous to those required for RhoA-GTP binding to human anillin. These RBD mutations, either alone or in combination (the double mutant henceforth designated as RBD*), abrogated the ability of the Anillin-ΔN or full-length Anillin to recruit Sep2 to cleavage furrows during cytokinesis (Figures 1F, 1G, and Video S2, quantified in Figure 1J). A failure of Anillin-RBD*-mCherry to recruit

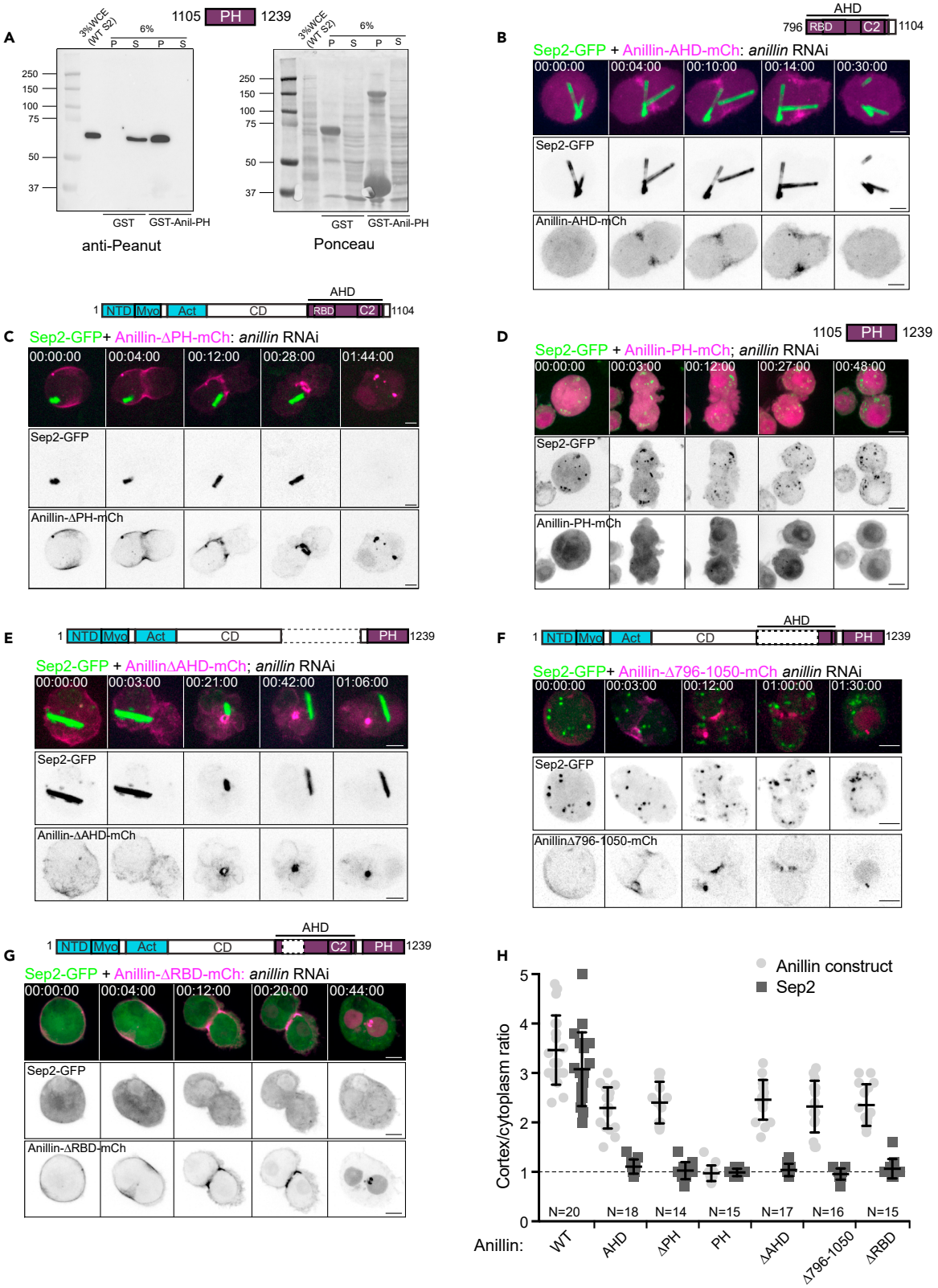
A
1105 PH 1239
3%WCE (WT S2)
6%
P S P S
250
150
100
75
50
37
GST
GST-Anil-PH
anti-Peanut
Ponceau
B
AHD
796 RBD C2 1104
Sep2-GFP + Anillin-AHD-mCh: anillin RNAi
00:00:00
00:04:00
00:10:00
00:14:00
00:30:00
Sep2-GFP
Anillin-AHD-mCh
C
1 NTD Myo Act CD RBD C2 1104
Sep2-GFP+ Anillin-ΔPH-mCh: anillin RNAi
00:00:00
00:04:00
00:12:00
00:28:00
01:44:00
Sep2-GFP
Anillin-ΔPH-mCh
D
1105 PH 1239
Sep2-GFP + Anillin-PH-mCh; anillin RNAi
00:00:00
00:03:00
00:12:00
00:27:00
00:48:00
Sep2-GFP
Anillin-PH-mCh
E
1 NTD Myo Act CD PH 1239
Sep2-GFP + AnillinΔAHD-mCh; anillin RNAi
00:00:00
00:03:00
00:21:00
00:42:00
01:06:00
Sep2-GFP
Anillin-ΔAHD-mCh
F
AHD
1 NTD Myo Act CD PH 1239
Sep2-GFP+ Anillin-Δ796-1050-mCh anillin RNAi
00:00:00
00:03:00
00:12:00
01:00:00
01:30:00
Sep2-GFP
AnillinΔ796-1050-mCh
G
AHD
1 NTD Myo Act CD C2 PH 1239
Sep2-GFP + Anillin-ΔRBD-mCh: anillin RNAi
00:00:00
00:04:00
00:12:00
00:20:00
00:44:00
Sep2-GFP
Anillin-ΔRBD-mCh
H
Anillin construct
Sep2
Cortex/cytoplasm ratio
5
4
3
2
1
0
N=20
N=18
N=14
N=15
N=17
N=16
N=15
Anillin:
WT
AHD
ΔPH
PH
ΔAHD
Δ796-1050
ΔRBD

Figure 2. The PH domain of Anillin binds septins but is insufficient for recruiting septins to the furrow, which also requires a functional RBD

(A) Pull-down of endogenous septin complexes from whole cell extracts (WCE) of S2 cells by recombinant GST or GST-Anillin-PH. Pellet (P) and supernatant (S) fractions were separated by SDS-PAGE, transferred to membranes and immunoblotted with anti-Peanut antibody (left panel). Right panel shows Ponceau-S staining of the transferred proteins before blotting. Note that GST was run off the bottom of the gel.

(B and C) Time-lapse sequences of transiently transfected S2 cells co-expressing Septin2-GFP and either Anillin-AHD-mCherry (B) or Anillin-ΔPH-mCherry (C), following Anillin RNAi.

(D–G) Time-lapse sequences of S2 cells co-expressing Septin2-GFP and Anillin-PH-mCherry (D), or Anillin-ΔAHD-mCherry (E), or Anillin-Δ796-1050-mCherry (F) or Anillin-ΔRBD-mCherry (G).

(H) Quantification of cortical enrichment of transiently expressed Septin2-GFP and indicated mCherry-tagged Anillin constructs following endogenous Anillin RNAi. Normalized cortex/cytoplasmic intensity ratios obtained from line profile measurements of cells during mid-furrowing are shown for N = 14–20 cells per condition, from 3 independent experiments. Bars represent mean values and SD. Times are h:min:s and scale bars are 5 μm. See also Figure S2.

Sep1-GFP to the cleavage furrow was also observed, although in this case Sep1-GFP decorated the later midbody microtubules either side of the furrow (Figure S1F). These data indicate that Rho1-GTP binding to the Anillin RBD is required for Sep1 and Sep2 recruitment to the cleavage furrow. The RBD mutations also prevented the furrow localization of the Anillin C-terminus (Anillin-ΔN-RBD*, see quantification in Figure 1J), confirming that Rho1-GTP binding is also necessary to recruit the Anillin AH-PH region to the furrow.

We previously showed that Rho1, Anillin and Pnut form tubulo-filamentous, membrane-associated structures when cytokinesis initiates under conditions where actin polymerization is inhibited using Latrunculin A (LatA).[9] Characterizing these "LatA structures" led to the initial proposal of a separate Rho1-dependent pathway, distinct from actomyosin,[39] which forms the basis of what we recently named the "anillo-septin" sub-network.[16] In the present study, we sought to test the ability of Anillin RBD mutants to assemble anillo-septin-dependent LatA structures. RBD mutations abolished the ability of full-length Anillin-mCherry to localize to the equatorial plasma membrane and to recruit Sep2-GFP during anaphase in LatA (Figures 1H and 1I). This further supports the conclusion that Rho1-GTP binding to the Anillin RBD within the AH domain is required for septin recruitment to the furrow. It also further validates the LatA structures as a valuable readout of anillo-septin assembly, independent of actomyosin.[9] Finally, because the Rho1-dependent recruitment of wild-type Anillin persists even in the absence of F-actin, it supports the conclusion that anillo-septin assembly occurs directly at the plasma membrane. This supports the inference that the normal localization pattern of Anillin at cleavage furrows includes at least 2 pools: (1) F-actin-dependent Anillin, which localizes via its N-terminus and is LatA-sensitive; and (2) membrane-associated anillo-septin, which localizes via its Rho1-GTP-bound C-terminus and is LatA-resistant.

The PH domain of anillin recruits septins to the furrow, but only in the presence of a functional RBD

Prior studies showed that septins interact with the human ANLN PH domain.[21,22] Consistent with this, we found that a recombinant Anillin PH domain fused to glutathione-S-transferase (GST) was sufficient to robustly pull-down endogenous Pnut from untransfected S2 cell lysates, unlike control GST alone (Figure 2A). This confirms that the PH domain is sufficient to bind, directly or indirectly, Pnut, which forms the central dimer of the *Drosophila* septin hexamer. To test the requirement for the Anillin PH domain in recruiting septins to the furrow, we examined mCherry-tagged Anillin constructs lacking the PH domain. Although at lower levels than wild-type Anillin, the Anillin AH domain (Figure 2B) and Anillin-ΔPH (Figure 2C) were each recruited to the furrows of cells depleted of endogenous Anillin, but in both cases there was no accompanying cortical enrichment of Sep2-GFP (quantified in Figure 2H), a marker for the hexameric septin complex. These data indicate that the Anillin PH domain is required for the furrow localization of septins, consistent with previous studies of the human Anillin PH domain.[21,22] The ability of the AH domain alone to localize to furrows suggests that the RBD-dependent recruitment of the Anillin AH domain occurs independently of septins (Figure 2B).

We next sought to test whether the PH domain of Anillin is sufficient to recruit septins to the cortex. When expressed alone, the mCherry-tagged PH domain was diffusely cytoplasmic and thus unable to recruit septins to the plasma membrane of dividing S2 cells (Figure 2D). However, no cortical septin enrichment was observed even when the PH domain was grafted onto the Anillin N-terminus, i.e. in the context of Anillin-ΔAHD (Figures 2E and 2H), which could still localize to the actomyosin network of the furrow through its intact N-terminus.[38]

It was previously shown that the human PH domain, when extended 56 amino acids into the AH domain, could recruit septins to ectopic structures at the plasma membrane of HeLa cells.[22] We generated an orthologous extension of the *Drosophila* PH domain (amino acids 1051–1239) and found that it localized to puncta in the cytoplasm, which Sep2 partially colocalized with (Figure S2A), but it still did not recruit septins to the plasma membrane, either alone, or when grafted onto the Anillin N-terminus (i.e. Anillin-Δ796–1050, Figures 2F and 2H), which clearly localized to the furrow cortex. Further extensions of the PH domain into the AH domain, even including all of the AH domain except the RBD (Anillin-ΔRBD, Figure 2G) also failed to restore the ability to recruit septins to the furrow (Figures S2B and S2C). We therefore conclude that the recruitment of septins to the cleavage furrow requires both the Anillin PH domain and the Rho1-GTP binding-competent AH domain. Because the AH domain alone could itself localize to the furrow (Figure 2B), its binding to Rho1-GTP must occur first and as a pre-requisite for subsequent septin recruitment via the PH domain.

Recruited septins exert positive feedback to enhance the localization of the anillin C-terminus at the furrow

We tested for a potential reciprocal contribution of septins in promoting Anillin localization. Because the C-terminal AH and PH domains (i.e., Anillin-ΔN) localized robustly to the furrow and recruited the septins without the confounding influence of the Anillin N-terminal interactions with the actomyosin network, we examined constructs comprising these domains. Depletion of Sep2 significantly reduced the furrow cortex: cytoplasm ratio of Anillin-ΔN, by approximately 50% (Figure 3A, quantified in Figure 3D, $p<0.001$). However, Sep2 depletion did not alter the furrow cortex: cytoplasm ratios of the AH domain alone (Figures 3B and 3D), confirming that the AHD is recruited independently of Sep2. The degree of cortical enrichment of the AH domain alone was similar to that of Anillin-ΔN following Sep2 RNAi. Unsurprisingly, Sep2 depletion had no effect on the localization patterns of Anillin-ΔN-RBD*, a negative control that failed to be recruited to the furrow (Figures 3C and 3D). We previously showed that, like *sep2* RNAi, *pnut* RNAi also inhibits the furrow localization of Anillin-ΔN.[38] Because loss of one septin can disrupt the stability of others in the complex,[35,40–42] it is expected that the whole septin complex is disrupted in both cases. Besides Sep1, Sep2, and Pnut, the *Drosophila* genome also encodes Sep4 and Sep5. Sep4 is within the same phylogenetic sub-group as Sep1 and thus, according to the Kinoshita rule,[43] potentially interchangeable with Sep1. Sep5 is a partially redundant retrogene copy of Sep2.[44] However, Sep4 and Sep5 were not studied here as our prior observations found no phenotypes from dsRNAs targeting them in S2 cells.[45] Nevertheless, the current data reinforce the conclusion that detectable Rho1-dependent recruitment of the Anillin AH domain to the cleavage furrow can occur independently of Sep2, Pnut, and of the PH domain. However, once recruited by the entire AH-PH domain, these septins exert positive feedback to enhance or sustain the localization of the Anillin C-terminus at the furrow. Furthermore, because the Rho1-dependent localization of septins persists in the absence of F-actin (i.e., in LatA, Figure 1H and[9]), we infer that this feedback mechanism occurs directly at the furrow plasma membrane.

Rho1-dependent anillo-septin assembly is required for timely CR closure and its faithful transition to the midbody ring

We next assessed the functional consequences to cytokinesis of mutations that specifically perturbed anillo-septin assembly, but not actomyosin assembly or scaffolding, once again using live-cell imaging. Control cells induced to express wild-type Anillin-GFP (Figure 4A), invariably closed their CRs within 10 min of anaphase onset (Figure 4C) and 0% underwent furrow regression during at least 2 h of imaging post-furrowing (Figure 4D). Conversely, cells expressing Anillin-RBD*-GFP (Figure 4B), which localizes to the actomyosin sub-network but is unable to recruit septins or to associate with the plasma membrane (as evidenced in LatA), exhibited significantly slowed CR closure, taking 7 min to close halfway instead of the usual 3–4 min (Figure 4C). This slowed closure was often accompanied by excessive blebbing of the furrow plasma membrane (as in Figure 4B, 00:03:30 timepoint, see also Video S3), a phenotype consistent with cortical instability that has been noted in numerous prior studies of the loss of Anillin function.[9–11,38,46–48] After protracted closure, Anillin-RBD*-dependent CRs invariably lost their attachment to the plasma membrane and, in 100% of observed cases, regressed to yield binucleate cells (Figure 4D). A common feature of cells expressing wild-type Anillin-GFP was shedding from the late CR/nascent midbody ring (Figures 4A and 4E), a septin-dependent phenomenon that we previously described.[49] Cells expressing Anillin-RBD* mutant displayed no evidence of shedding from the late CR (Figures 4B and 4E). Rather, Anillin-RBD* localized to prominent midbody ring-like structures that persisted in the cytoplasm of the binucleate cells after furrow regression (Figure 4F). These internal midbody ring-like structures were observed in 91% of failed

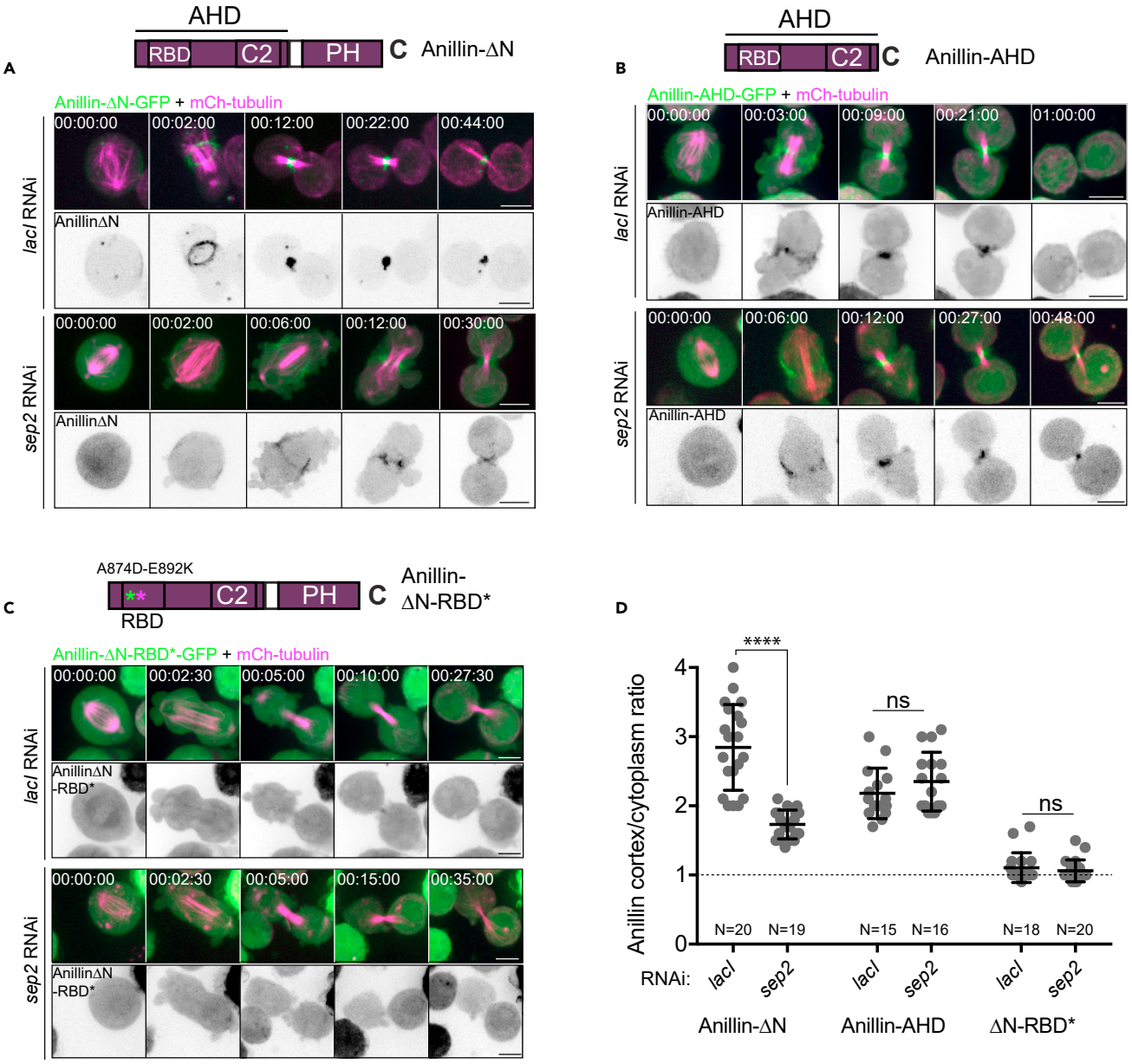

Figure 3. Recruited septins exert positive feedback to enhance the localization of the Anillin C-terminus at the furrow

(A–C) Representative, high-resolution time-lapse sequences of transiently transfected S2 cells after 7-day of control *lacI* RNAi (top panels) or *sep2* RNAi (bottom panels), constitutively expressing mCherry-tubulin (magenta) and inducibly expressing either Anillin-ΔN-GFP (A, green or inverted grayscale), or Anillin-AHD-GFP (B, green or inverted grayscale), or AnillinΔN-RBD* (C, green or inverted grayscale).

(D) Quantification of mid-furrowing cortex: cytoplasm ratios of the indicated Anillin-GFP constructs following 7 days of control *lacI* or *sep2* RNAi, showing that *sep2* RNAi significantly reduces (but does not abolish) the furrow localization of Anillin-ΔN, while *sep2* RNAi does not affect the furrow localization of Anillin-AHD or Anillin-RBD*. Bars represent mean and SD, **** refers to $p<0.001$; ns, not significant. Scale bars, 5 μm.

cytokinesis attempts and persisted over several hours (Figure 4F). They resembled the internal structures we previously reported with the Anillin-ΔC-GFP construct,[38] although in the current study they tended to be more open rings (C-shaped) rather than closed rings (quantified in Figure 4F). Similar to Anillin-ΔC,[38] these internal ring structures resembled mature midbody rings in that they contained the Citron kinase, Sticky, myosin ($MRLC^{sqh}$) and RacGAP50C/Tumbleweed but were devoid of the septins (Sep2 and Peanut) and F-actin (Figure S3). These similarities between Anillin-RBD* and Anillin-ΔC suggest that the RBD* mutant may effectively behave as a C-terminal null allele, and that Rho1-GTP binding activates the C-terminus.

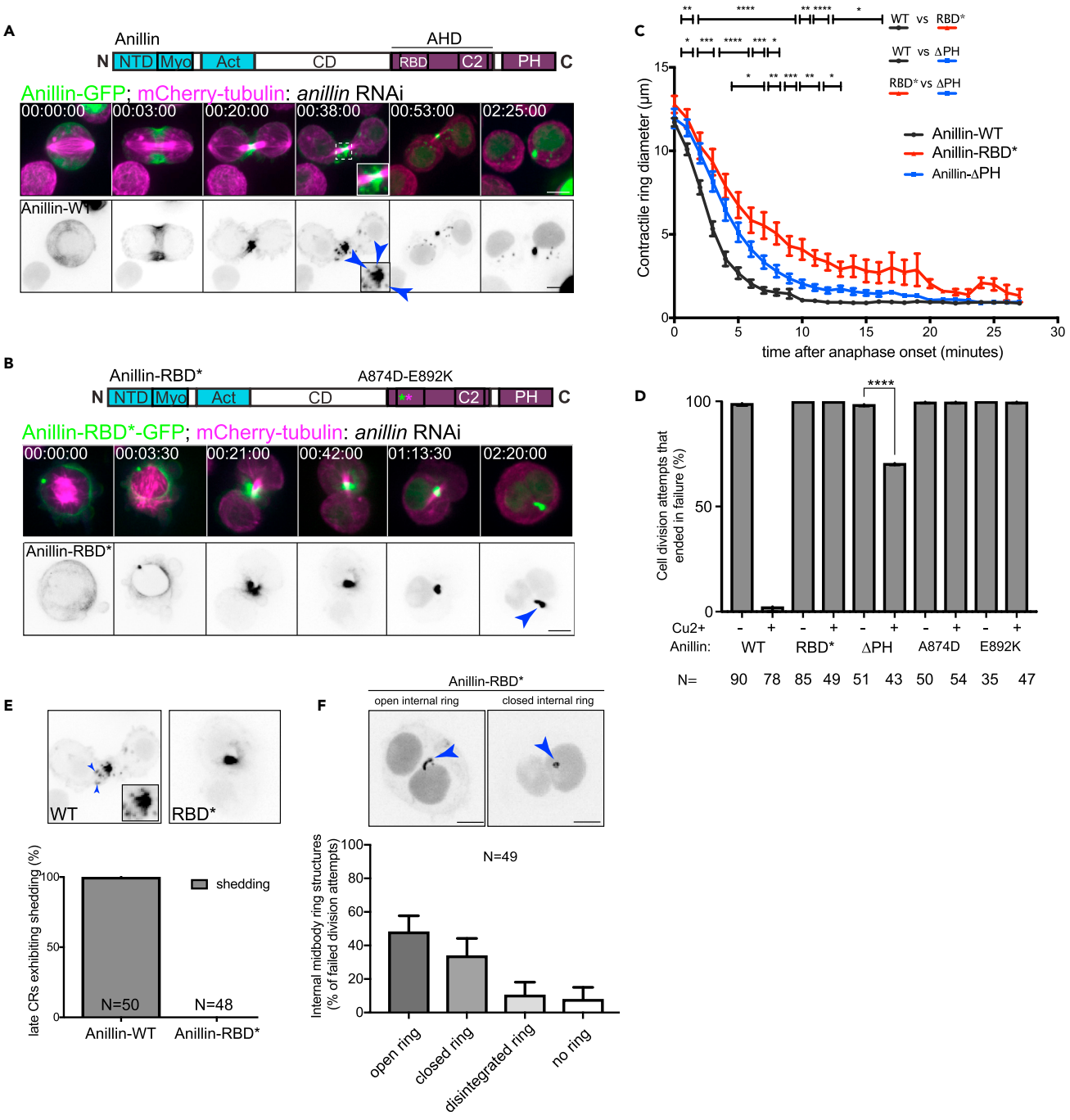

Figure 4. Rho1-dependent anillo-septin assembly is required for timely CR closure and its faithful transition to the midbody ring

Representative time-lapse sequences of S2 cells transiently transfected to constitutively express mCherry-tubulin and inducibly express Anillin-GFP (A) or AnillinRBD*-GFP (B), during 3 days of anillin RNAi. Arrowheads in A show shed particles, arrowhead in B shows failed midbody ring-like structure.

(C) Measurements of CR diameter over time from cells that were dependent on Anillin-WT (black), Anillin-RBD* (red) or Anillin-ΔPH (blue), following 3 days of Anillin RNAi. Mean values ±SD are shown for N = 25 cells per condition and n = 3 independent experiments. Conditions were compared by unpaired t-test, with all statistically significant differences shown for the different time periods, with p values <0.05 (*), <0.01 (**), <0.001 (***), or <0.0001 (****).

(D) Quantification from time-lapse recordings of cell division attempts that resulted in binucleate cells, following depletion of endogenous Anillin and induced expression of indicated Anillin constructs (N = 35–90 per condition).

(E) Quantification of late CRs that showed evidence of shedding of either Anillin-GFP or Anillin-RBD*-GFP (N = 48–50 division attempts per condition).

(F) Quantification from time-lapse recordings of the phenotypic outcomes of failed division attempts of CRs that were dependent on Anillin-RBD*-GFP.

Scale bars, 5 μm. See also Figure S3.

In cells expressing Anillin-ΔPH-GFP, and depleted of endogenous Anillin, CRs closed at an intermediate rate that was slower than control Anillin-GFP-dependent CRs, but faster than Anillin-RBD*-dependent CRs (Figure 4C). 70% of these Anillin-ΔPH-dependent division attempts failed (Figure 4D, 30 from 43 attempts), resulting in binucleate cells that also harbored internal midbody ring-like structures (not shown), whereas the 30% that succeeded represent partial rescue (13 from 43 attempts). The intermediate phenotype of Anillin-ΔPH, both in terms of the rate of CR closure (Figure 4C) and the frequency of cytokinesis failure (Figure 4D), suggests that Anillin-ΔPH, which retains a functional RBD, is more functional than Anillin-RBD*.

We conclude that the Rho1-GTP-binding competent AH domain provides some functionality to Anillin that is independent of septin recruitment, but that it is also a pre-requisite for septin co-recruitment, which additionally requires the Anillin PH domain. We further conclude that Rho1-GTP binding to Anillin, and subsequent anillo-septin assembly, are both required for timely CR closure and a faithful transition of the CR to the midbody ring.

Anillo-septin assembly and function is conserved in human cells

To test whether RhoA-GTP-bound ANLN is also required for septin recruitment in human cells, we assayed the furrow recruitment of SEPT6, SEPT2 and SEPT7, the hexamer-forming orthologs of *Drosophila* Sep2, Sep1, and Pnut, respectively, and of SEPT9, which forms the central dimer of mammalian septin octamers.[29–31] Although all four of these mammalian septins localized to the furrows of HeLa cells in the presence of endogenous ANLN, their furrow localization patterns were lost on siRNA-mediated depletion of ANLN (Figures 5A, 5B, and S4). Expression of wild-type siRNA-resistant GFP-tagged ANLN restored SEPT9 localization to the furrow, confirming that septin recruitment in HeLa cells is also ANLN-dependent (Figure 5C), consistent with a previously published report.[21] However, in agreement with our findings from *Drosophila* S2 cells, a single point mutation (A703E) in the ANLN RBD that was shown to eliminate ANLN-RhoA-GTP binding *in vitro*,[23] abolished the furrow recruitment of SEPT9, assessed following depletion of endogenous ANLN (Figures 5D and 5E). Furthermore, ANLN-A703E was unable to rescue cytokinesis failure after RNAi-mediated depletion of ANLN (100% failure, Figure 5F). We therefore conclude that the RhoA-dependent recruitment of septins to the CR, as well as the functional importance of anillo-septin assembly for cytokinesis, is conserved between *Drosophila* S2 cells and human HeLa cells.

DISCUSSION

Despite more than 50 years of intensive research, the mechanisms of assembly, closure and disassembly of cytokinetic CRs remain incompletely understood. The small GTPase RhoA has emerged as the master regulator of the CR of animal cells and considerations of RhoA-dependent actomyosin assembly and contractility have naturally come to dominate current views of CR function. However, the experiments described here highlight the fact that active RhoA also controls the recruitment and assembly of an additional, independently membrane-anchored, and experimentally separable network of the contractile ring. This non-canonical "anillo-septin" network co-exists alongside the canonical actomyosin network at the cleavage furrow and is also required for proper CR closure (Figure 6A).

Septins are long-known components of cleavage furrows,[50] but their mechanisms of localization, their relationship with the actomyosin cytoskeleton and their precise roles in the cleavage process all remain unclear. Indeed, septins appear dispensable for cytokinesis in some contexts, whereas essential in others.[41,51,52] Prior studies have shown that septin recruitment depends on Anillin.[9,21,33,34] However, the fact that septins can also interact with F-actin and myosin II,[36,37] gives rise to multiple possibilities for how septins might be recruited to the CR in an Anillin-dependent manner. The current study clearly demonstrates that the actomyosin network is unable to recruit septins even when scaffolded by a fully functional Anillin N-terminus, in both fly S2 cells and human HeLa cells. This implies that neither the documented ability of F-actin and fly septins to co-polymerize *in vitro*,[36] nor the interaction between mammalian septins and myosin II,[37] contribute to the recruitment of septins to the CR. Rather, septin recruitment to the CR appears to uniquely and specifically require the Anillin C-terminus, which must be both: (1) competent to bind active RhoA-GTP, and (2) contain its PH domain (Figure 6A). Furthermore, this septin recruitment mechanism appears to occur directly at the plasma membrane, as it persists in the absence of an F-actin cortex and myosin II.[9] The results are consistent with prior studies showing that the human ANLN PH domain binds septins and is required for their localization.[21,22] However, they further show that the adjacent Rho1-bound

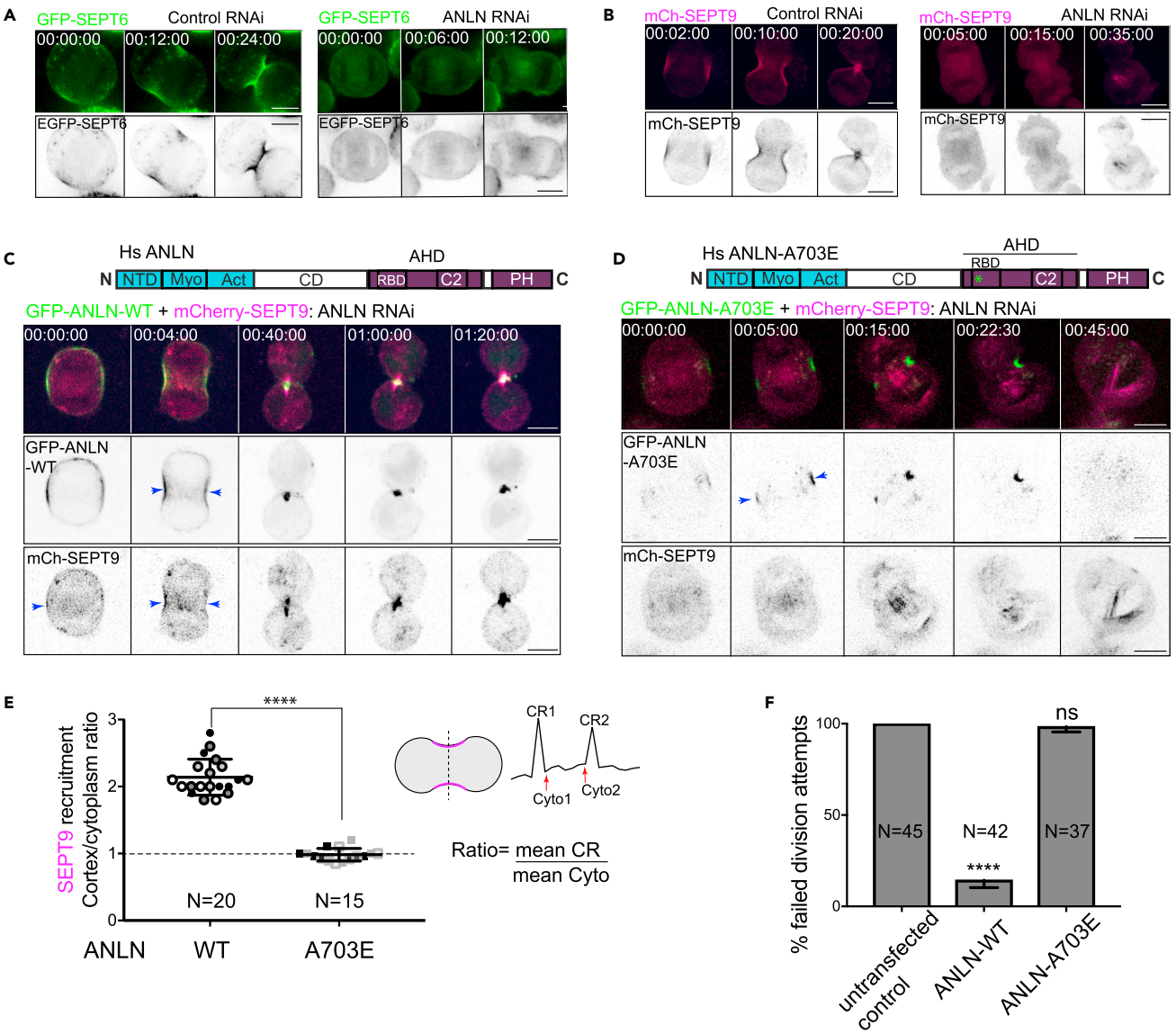

Figure 5. RhoA-dependent anillo-septin assembly and function is conserved in human cells

(A and B) Representative time-lapse sequences of dividing HeLa cells transiently expressing GFP-SEPT6 (A) or mCherry-SEPT9 (B), following control (left panels) or ANLN depletion (right panels).

(C and D) Representative time-lapse sequences of dividing HeLa cells transiently expressing mCherry-SEPT9 and siRNA-resistant GFP-ANLN-WT (C) or GFP-ANLN-A703E (D), following depletion of endogenous ANLN.

(E) Quantification of cortex: cytoplasm ratios of mCherry-SEPT9 at the CRs of cells expressing ANLN-WT or ANLN-A703E. Data are from 3 independent experiments, each shaded differently. Total number of cells analyzed (*N*) is indicated on the respective bars and error bars represent SD between experiments. ****, p = 0.0002, t-test.

(F) Quantification of failed division attempts scored from time-lapse recordings of 3 independent experiments. Total number of cells analyzed (*N*) is indicated on the respective bars and error bars represent SD between experiments. ****, p = 0.00015, t-test. Scale bars, 5 μm. See also Figure S4.

AH domain is a pre-requisite for PH-domain-dependent septin recruitment and that both events are required for timely furrow ingression.

The simplest model is that Rho1-GTP binding to the Anillin RBD relieves autoinhibition of the PH domain allowing it to bind and recruit the septins. However, this model cannot account for the observation that Anillin-ΔRBD fails to recruit septins. The Rho1-GTP-bound AH domain must therefore be more directly involved in the septin recruitment process together with the PH domain. We speculate that the robust

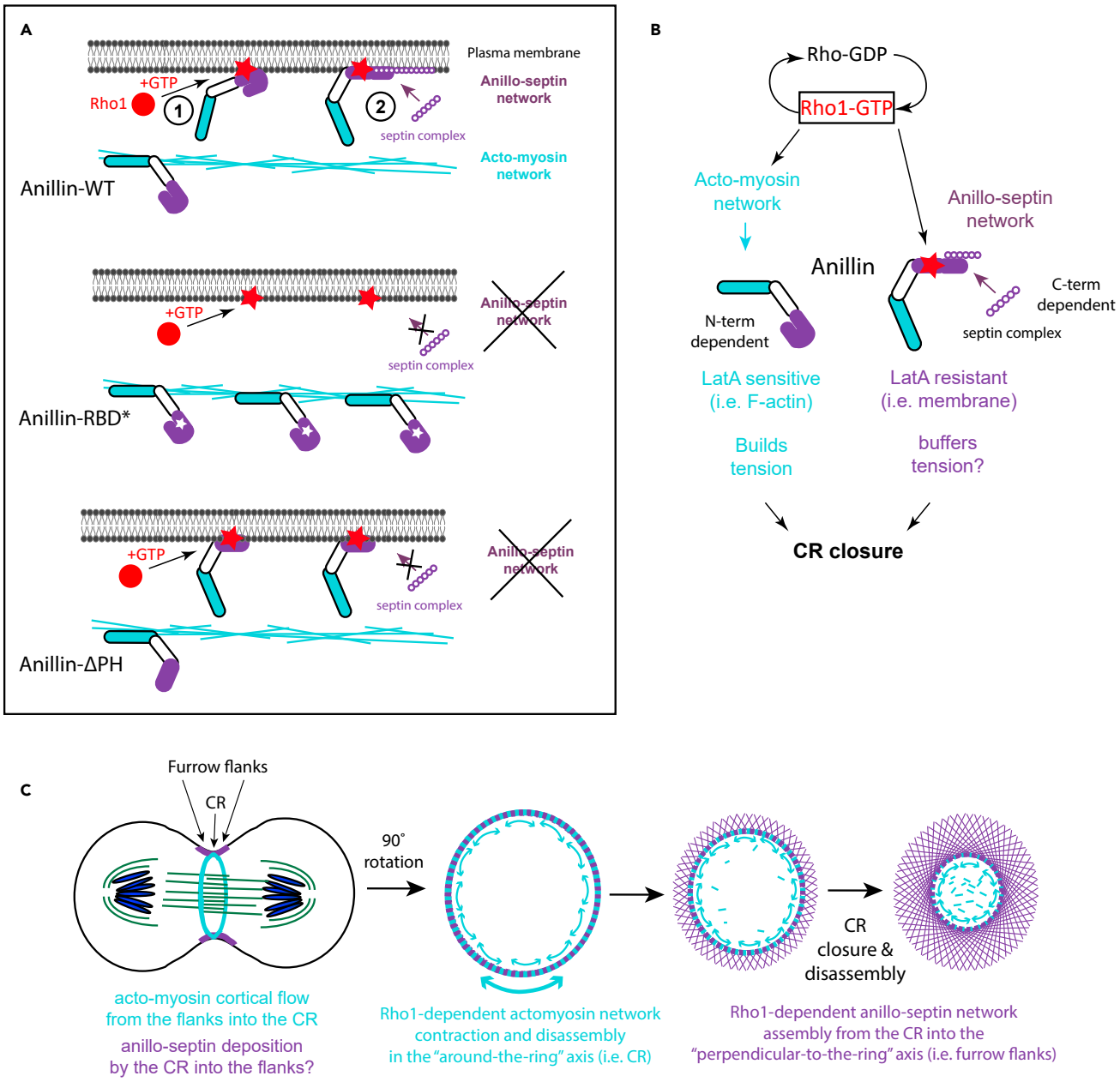

Figure 6. Summary of data and speculative model for how the Rho1-dependent anillo-septin network may be coordinated with the actomyosin network during CR closure

(A) Summary of data regarding the recruitment of septins and Anillin to the furrow cortex in the context of wild-type Anillin, Anillin-RBD* and Anillin-ΔPH mutants.

(B) Model for how Rho1-dependent actomyosin and anillo-septin networks may be integrated with one another to promote contractile ring closure. Rho1-GTP assembles the canonical actomyosin network, which Anillin molecules scaffold via their N-termini to promote CR tension. However, Rho1-GTP also recruits Anillin molecules via their C-termini to the plasma membrane where they assemble the non-canonical anillo-septin network, independently of actomyosin. Both networks are required for proper CR closure.

(C) Speculative model for how separation of actomyosin and anillo-septin networks may buffer CR tension and promote CR closure. As the actomyosin network constricts in the around-the-ring axis, the anillo-septin network grows out from the CR into the flanks of the furrow, in the perpendicular-to-the-ring axis. As anillo-septin assembles, it sequesters Rho1-GTP and associated membrane away from the actomyosin sub-network of the constricting CR, thereby promoting local actomyosin sub-network disassembly and a concomitant shortening of the around-the-ring axis of the CR. Anillo-septin-sequestered Rho1-GTP may then be re-released in the furrow flanks to power actomyosin-dependent cortical flow back into the CR in a positive-feedback loop that sustains tension at the CR, while progressively shortening its ring axis.

septin localization observed with a functional Anillin C-terminus involves septin polymerization and/or a higher order assembly process in which Rho1-GTP, the AH and the PH domains all participate, together with the appropriate plasma membrane lipid environment. In this regard, the ANLN AH domain harbors a membrane-binding, cryptic C2 domain,[23] that has been proposed to concentrate PI(4,5)P2 to sustain RhoA-GTP.[53] PI(4,5)P2 also promotes septin filament assembly.[54] The PH domain of ANLN also binds PI(4,5)P2,[21] but this activity alone is insufficient to mediate septin recruitment, as elegantly shown by Liu et al.,[21] who replaced the human ANLN PH domain with the PH domain of PLCδ (which also binds PI(4,5)P2) and showed that this chimera restored membrane localization to Anillin but not the co-recruitment of septins to the furrows of HeLa cells. It thus seems likely that assembly of the anillo-septin network requires the coincidence of multiple events: direct Rho1-GTP-Anillin RBD interactions; septin-Anillin PH domain interactions; and PI(4,5)P2 interactions with septins, the Anillin C2 and PH domains. Although our observations clearly show that Rho1/RhoA binding to Anillin/ANLN is required for the recruitment of septins to the furrows of fly S2 cells and human HeLa cells, respectively, there may some subtle differences between these two cell types. In agreement with the current study, Sun et al.[23] found that the *Drosophila* AHD localized less well than the AH-PH region (i.e. Anillin-ΔN). However, the analogous human AHD did not localize at all to furrows.[23] Yet, Budnar et al.[53] showed that the human AHD alone is clearly able to at least partially localize and function in MCF-7 cells.

In our hands, the *Drosophila* Anillin AH-PH region (i.e. Anillin-ΔN) was sensitive to RNAi of *sep2* (Figure 3) or *pnut*[38] and it was recruited to the equatorial cortex more robustly than the AH domain alone (Figure 3). This suggests that, once recruited, the septins feedback to enhance the localization of the Anillin C-terminus (and presumably Rho1-GTP) at the plasma membrane. This feedback could involve the well documented ability of septin filaments to laterally compartmentalize membranes and act as membrane diffusion barriers.[27] For example, newly assembled septin filaments could locally restrict the diffusion of PI(4,5)P2, thereby prolonging the lifetime of Rho1-GTP.

We first proposed the existence of an actomyosin-independent, septin-based sub-network of the CR in prior work showing that Rho1 activation in the presence of LatA drives Rho1, Anillin and septin co-recruitment in tubular structures at the equatorial plasma membrane.[9] The current study reinforces and extends this to clearly show that this membrane-associated anillo-septin assembly mechanism occurs via the Anillin C-terminus (Figures 6A and 6B). Conversely, the ability of the Anillin N-terminus to localize with the actomyosin network requires an intact F-actin cortex, because the cortical localization of Anillin-RBD* is abolished in LatA (Figures 6A and 6B). Nanoscopy of the *Schizosaccharomyces pombe* CR revealed three distinct layers wherein F-actin occupies the most membrane-distal layer, while the septins and the Anillin-like Mid1 occupy the most membrane-proximal layer.[55] Thus, the two separable actions of Anillin (N-terminal actomyosin scaffolding versus C-terminal septin scaffolding) may occur at two distinct cortical layers of the S2 cell CR (Figures 6A and 6B). Further studies are required to determine whether individual Anillin molecules can associate with actomyosin and septin networks at the same time (i.e., spanning them) or whether Anillin can only associate with one network or the other in a mutually exclusive manner.

Through its N-terminus, Anillin can cross-link actin filaments to generate force,[13–15] and can also bind myosin II.[11] These actomyosin scaffolding roles of Anillin presumably promote CR assembly and the generation of tension. Nevertheless, the Anillin-RBD* mutant clearly reveals that the ability to scaffold actomyosin is insufficient to promote timely CR closure. In the absence of Rho1-GTP binding to the Anillin C-terminus, anillo-septin assembly is completely blocked and furrowing is slow and incomplete.

Why does furrowing require two Rho1-dependent cytoskeletal networks?

The seminal work of Schroeder 50 years ago revealed that the circumference and volume of the CR (which includes both cytoskeleton and membrane) progressively shrink as the CR closes and disassembles.[7] We have since learned that the actomyosin cytoskeleton is also constantly being reeled into the closing CR via cortical flow in the perpendicular-to-the-ring axis. This cortical flow must be accompanied by an inflow of actomyosin-anchored membrane, which presents a paradox: How can the volume of the CR membrane progressively shrink in the ring axis if membrane is continually flowing in the perpendicular axis, via cortical flow, from both sides of the furrow? As Schroeder surmised,[56] membrane must also be flowing out of the CR into the flanks of the furrow. The septin cytoskeleton, with its ability to laterally compartmentalize the plasma membrane,[27] is an ideal candidate to facilitate such a process. We speculate that as the actomyosin cytoskeleton constricts in the around-the-ring axis, it transfers some of its membrane-associated Rho1 to the nascent anillo-septin network which is then

squeezed out into the perpendicular-to-the-ring axis (Figure 6C). According to this model,[16] assembling anillo-septin sequesters membrane-associated Rho1 (and Anillin) from the disassembling actomyosin network, promoting a shortening of the ring axis (i.e. CR closure). The slow closure of anillo-septin-defective furrows could thus reflect a reduced ability to translocate Rho1-GTP and membrane out of the ring axis and a concomitant slowed disassembly of the actomyosin network of the CR.

However, anillo-septin-defective CRs likely also close slowly because of reduced levels of active Rho1. Cortical RhoA staining is greatly diminished when Anillin is depleted,[10,53] suggesting that Anillin either promotes RhoA activation, or sustains active RhoA. The fact that Anillin-depleted furrows display high actomyosin contractility and furrow oscillations,[9–12] is inconsistent with a role for Anillin in RhoA activation. Rather, it is more likely that Anillin sustains the pool of active RhoA-GTP, presumably by inhibiting or delaying the GAP-stimulated inactivation of RhoA. Indeed, the AH domain of Anillin can prolong the membrane residency of RhoA-GTP and, through labile low affinity interactions, allows RhoA-GTP to toggle between Anillin and actomyosin effectors, independently of GEFs and GAPs.[53,57] We speculate that a nascent anillo-septin cytoskeletal network grows out from the CR into the perpendicular-to-the-ring axis (i.e., the furrow flanks), transiently sequestering Rho1-GTP away from the actomyosin network as it contracts at the CR. We further speculate that within the furrow flanks this transiently sequestered Rho1-GTP is released to re-activate actomyosin effectors (as per[53]), thereby driving cortical flow back into the CR. Such a putative positive feedback loop could sustain tension at the CR through cortical flow, while allowing the around-the-ring axis to progressively shorten. According to this speculative model, Anillin sustains high levels of active Rho1 which drives bidirectional membrane flow in the perpendicular-to-the-ring axis: inflow via RhoA-dependent actomyosin-driven cortical flow; and outflow via RhoA-dependent anillo-septin assembly. Ring closure could therefore proceed via a controlled and progressive (net) reduction in the volume of membrane in the around-the-ring axis,[7,56] driven by a rate of membrane outflow (facilitated by anillo-septin) that exceeds the rate of membrane inflow (driven by actomyosin).

It is also important to point out that Anillin likely impinges on the levels of cortical Rho1 in ways that are independent of direct binding of its RBD to Rho1-GTP. For instance, we have shown that the Anillin N-terminus binds the Citron kinase, Sticky, which itself also harbors a functional RBD.[18] We further showed that both the Anillin-Sticky interaction and a functional Sticky RBD are required for midbody ring formation, a process that begins during CR closure.[18] Preventing Rho1-GTP binding to the Anillin C-terminus (i.e., Anillin-RBD*) led to the formation of prominent internal midbody ring-like structures (this study), which likely depend on both Sticky-Anillin and Rho1-Sticky interactions.[18,49] Therefore Anillin-RBD* in this study likely stabilized Anillin N-terminus-Sticky and Sticky-Rho1-GTP interactions. The existence of different subpopulations of Rho1-GTP (bound to Anillin, or Sticky, or Diaphanous or Rho-kinase) makes it very challenging to deconvolve the full impact of Anillin on Rho1. In addition, Anillin can bind to components of the Rho1 activating complex: TUM/RacGAP50C in *Drosophila*,[58,59] or the RhoGEF, ECT2, in humans.[60] Such interactions may influence which RhoA target protein newly generated RhoA-GTP engages with. Evidently, much further work is needed to understand how all the components of the global RhoA-dependent network are coordinated with one another to control animal cell cytokinesis. However, the anillo-septin network described here must be considered as an integral part of that global network.

Limitations of the study

The current study demonstrates that active Rho1 controls the recruitment of the Anillin C-terminus and the septins to the cleavage furrow and that this can occur independently of F-actin (i.e., directly at the plasma membrane in the presence of LatA) and in the absence of Anillin domains needed to interact with the actomyosin cytoskeleton (i.e., with Anillin-ΔN both in the presence and absence of LatA). It is logical to infer that active Rho1 recruits septins to the plasma membrane in the context of full-length wild-type Anillin in the presence of a fully functional actomyosin cytoskeleton, even if this is not shown directly. A key mechanistic question that the current study does not address is whether individual Anillin molecules can associate with actomyosin and RhoA/septins at the same time, or whether there are mutually exclusive pools. This latter possibility is attractive because it provides a plausible mechanism that could coordinate anillo-septin assembly with actomyosin disassembly to promote CR closure. Nevertheless, this model, together with that of anillo-septin deposition is the perpendicular-to-the-ring axis remains speculative from the current data. More sophisticated imaging analyses that simultaneously monitor actomyosin and septin components will be needed to understand how Anillin engages with each of these networks and the extent to which the two networks are coupled and/or uncoupled.

STAR★METHODS

Detailed methods are provided in the online version of this paper and include the following:

- KEY RESOURCES TABLE
- RESOURCE AVAILABILITY
  - Lead contact
  - Materials availability
  - Data and code availability
- EXPERIMENTAL MODEL AND STUDY PARTICIPANT DETAILS
  - Cell lines
- METHOD DETAILS
  - Molecular biology- cloning
  - S2 cell transfections and RNAi
  - HeLa cells transfection and RNAi
  - Live cell microscopy
  - Immunofluorescence microscopy
  - Image analysis (contractile ring closure and ratio of cortical versus cytoplasmic recruitment)
  - Recombinant protein expression
  - Whole cell extract preparation
  - GST pull down assay
  - Immunoblot
- QUANTIFICATION AND STATISTICAL ANALYSIS
  - Statistical analysis

SUPPLEMENTAL INFORMATION

Supplemental information can be found online at https://doi.org/10.1016/j.isci.2023.106903.

ACKNOWLEDGMENTS

We thank Dr Alisa Piekny (Concordia University, Montreal) for discussions, human Anillin constructs and reagents and Dr Elias Spiliotis, Drexel University, Philadelphia, PA, USA, for mammalian septin constructs. The Peanut (4C9H4) and Rho1 (p1D9) monoclonal antibodies described in[61,62] were obtained from the Developmental Studies Hybridoma Bank, created by the NICHD of the NIH and maintained at The University of Iowa, Department of Biology, Iowa City, IA 52242. We thank members of the Hickson laboratory and members of the laboratories of Abigail Gerhold, Greg Fitzharris and Jean-Claude Labbé for discussions. This research was supported by grants from the Canadian Institutes for Health Research (CIHR, MOP-97788 and PJT-183759), the Natural Sciences and Engineering Research Council (NSERC, RGPIN-2021-03324) and the Canadian Fund for Innovation (CFI) awarded to G.R.X.H. S.C.C. received a postdoctoral fellowship from the Sainte-Justine Foundation and G.R.X.H. received a senior scholarship from the Fonds de Recherche de Québec Santé (FRQS).

AUTHOR CONTRIBUTIONS

Conceptualization, G.R.X.H. and S.C.C.; Formal Analysis, S.C.C.; Investigation, S.C.C.; Writing–original draft, S.C.C.; Writing–Review and editing, G.R.X.H. and S.C.C.; Visualization, S.C.C.; Supervision, G.R.X.H.; Funding acquisition, G.R.X.H.

DECLARATION OF INTERESTS

The authors declare no competing interests.

INCLUSION AND DIVERSITY

One or more of the authors of this paper self-identifies as an underrepresented ethnic minority in their field of research or within their geographical location. We support inclusive, diverse, and equitable conduct of research.

Received: July 14, 2021
Revised: March 20, 2023
Accepted: May 12, 2023
Published: May 19, 2023

REFERENCES

1. Bement, W.M., Benink, H.A., and von Dassow, G. (2005). A microtubule-dependent zone of active RhoA during cleavage plane specification. J. Cell Biol. *170*, 91–101.

2. Basant, A., and Glotzer, M. (2018). Spatiotemporal regulation of RhoA during cytokinesis. Curr. Biol. *28*, R570–R580. https://doi.org/10.1016/j.cub.2018.03.045.

3. D'Avino, P.P., Giansanti, M.G., and Petronczki, M. (2015). Cytokinesis in animal cells. Cold Spring Harb. Perspect. Biol. *7*, a015834. https://doi.org/10.1101/cshperspect.a015834.

4. Green, R.A., Paluch, E., and Oegema, K. (2012). Cytokinesis in animal cells. Annu. Rev. Cell Dev. Biol. *28*, 29–58. https://doi.org/10.1146/annurev-cellbio-101011-155718.

5. Pollard, T.D., and O'Shaughnessy, B. (2019). Molecular mechanism of cytokinesis. Annu. Rev. Biochem. *88*, 661–689. https://doi.org/10.1146/annurev-biochem-062917-012530.

6. O'Shaughnessy, B., and Thiyagarajan, S. (2018). Mechanisms of contractile ring tension production and constriction. Biophys. Rev. *10*, 1667–1681. https://doi.org/10.1007/s12551-018-0476-6.

7. Schroeder, T.E. (1972). The contractile ring. II. Determining its brief existence, volumetric changes, and vital role in cleaving Arbacia eggs. J. Cell Biol. *53*, 419–434.

8. Pollard, T.D. (2017). Nine unanswered questions about cytokinesis. J. Cell Biol. *216*, 3007–3016. https://doi.org/10.1083/jcb.201612068.

9. Hickson, G.R.X., and O'Farrell, P.H. (2008). Rho-dependent control of anillin behavior during cytokinesis. J. Cell Biol. *180*, 285–294. https://doi.org/10.1083/jcb.200709005.

10. Piekny, A.J., and Glotzer, M. (2008). Anillin is a scaffold protein that links RhoA, actin, and myosin during cytokinesis. Curr. Biol. *18*, 30–36. https://doi.org/10.1016/j.cub.2007.11.068.

11. Straight, A.F., Field, C.M., and Mitchison, T.J. (2005). Anillin binds nonmuscle myosin II and regulates the contractile ring. Mol. Biol. Cell *16*, 193–201.

12. Goldbach, P., Wong, R., Beise, N., Sarpal, R., Trimble, W.S., and Brill, J.A. (2010). Stabilization of the actomyosin ring enables spermatocyte cytokinesis in Drosophila. Mol. Biol. Cell *21*, 1482–1493. https://doi.org/10.1091/mbc.E09-08-0714.

13. Field, C.M., and Alberts, B.M. (1995). Anillin, a contractile ring protein that cycles from the nucleus to the cell cortex. J. Cell Biol. *131*, 165–178.

14. Jananji, S., Risi, C., Lindamulage, I.K.S., Picard, L.P., Van Sciver, R., Laflamme, G., Albaghjati, A., Hickson, G.R.X., Kwok, B.H., and Galkin, V.E. (2017). Multimodal and polymorphic interactions between anillin and actin: their implications for cytokinesis. J. Mol. Biol. *429*, 715–731. https://doi.org/10.1016/j.jmb.2017.01.020.

15. Kučera, O., Siahaan, V., Janda, D., Dijkstra, S.H., Pilátová, E., Zatecka, E., Diez, S., Braun, M., and Lansky, Z. (2021). Anillin propels myosin-independent constriction of actin rings. Nat. Commun. *12*, 4595. https://doi.org/10.1038/s41467-021-24474-1.

16. Carim, S.C., Kechad, A., and Hickson, G.R.X. (2020). Animal cell cytokinesis: the rho-dependent actomyosin-anilloseptin contractile ring as a membrane microdomain gathering, compressing, and sorting machine. Front. Cell Dev. Biol. *8*, 575226. https://doi.org/10.3389/fcell.2020.575226.

17. Piekny, A.J., and Maddox, A.S. (2010). The myriad roles of Anillin during cytokinesis. Semin. Cell Dev. Biol. *21*, 881–891. https://doi.org/10.1016/j.semcdb.2010.08.002.

18. El-Amine, N., Carim, S.C., Wernike, D., and Hickson, G.R.X. (2019). Rho-dependent control of the Citron kinase, Sticky, drives midbody ring maturation. Mol. Biol. Cell *30*, 2185–2204. https://doi.org/10.1091/mbc.E19-04-0194.

19. Gai, M., Camera, P., Dema, A., Bianchi, F., Berto, G., Scarpa, E., Germena, G., and Di Cunto, F. (2011). Citron kinase controls abscission through RhoA and anillin. Mol. Biol. Cell *22*, 3768–3778. https://doi.org/10.1091/mbc.E10-12-0952.

20. Madaule, P., Eda, M., Watanabe, N., Fujisawa, K., Matsuoka, T., Bito, H., Ishizaki, T., and Narumiya, S. (1998). Role of citron kinase as a target of the small GTPase Rho in cytokinesis. Nature *394*, 491–494. https://doi.org/10.1038/28873.

21. Liu, J., Fairn, G.D., Ceccarelli, D.F., Sicheri, F., and Wilde, A. (2012). Cleavage furrow organization requires PIP(2)-mediated recruitment of anillin. Curr. Biol. *22*, 64–69. https://doi.org/10.1016/j.cub.2011.11.040.

22. Oegema, K., Savoian, M.S., Mitchison, T.J., and Field, C.M. (2000). Functional analysis of a human homologue of the Drosophila actin binding protein anillin suggests a role in cytokinesis. J. Cell Biol. *150*, 539–552.

23. Sun, L., Guan, R., Lee, I.J., Liu, Y., Chen, M., Wang, J., Wu, J.Q., and Chen, Z. (2015). Mechanistic insights into the anchorage of the contractile ring by anillin and Mid1. Dev. Cell *33*, 413–426. https://doi.org/10.1016/j.devcel.2015.03.003.

24. Beaudet, D., Pham, N., Skaik, N., and Piekny, A. (2020). Importin binding mediates the intramolecular regulation of anillin during cytokinesis. Mol. Biol. Cell *31*, 1124–1139. https://doi.org/10.1091/mbc.E20-01-0006.

25. Beise, N., and Trimble, W. (2011). Septins at a glance. J. Cell Sci. *124*, 4141–4146. https://doi.org/10.1242/jcs.087007.

26. Mostowy, S., and Cossart, P. (2012). Septins: the fourth component of the cytoskeleton. Nat. Rev. Mol. Cell Biol. *13*, 183–194. https://doi.org/10.1038/nrm3284.

27. Caudron, F., and Barral, Y. (2009). Septins and the lateral compartmentalization of eukaryotic membranes. Dev. Cell *16*, 493–506. https://doi.org/10.1016/j.devcel.2009.04.003.

28. Field, C.M., al-Awar, O., Rosenblatt, J., Wong, M.L., Alberts, B., and Mitchison, T.J. (1996). A purified Drosophila septin complex forms filaments and exhibits GTPase activity. J. Cell Biol. *133*, 605–616.

29. Mendonça, D.C., Macedo, J.N., Guimarães, S.L., Barroso da Silva, F.L., Cassago, A., Garratt, R.C., Portugal, R.V., and Araujo, A.P.U. (2019). A revised order of subunits in mammalian septin complexes. Cytoskeleton (Hoboken) *76*, 457–466. https://doi.org/10.1002/cm.21569.

30. Soroor, F., Kim, M.S., Palander, O., Balachandran, Y., Collins, R.F., Benlekbir, S., Rubinstein, J.L., and Trimble, W.S. (2021). Revised subunit order of mammalian septin complexes explains their in vitro polymerization properties. Mol. Biol. Cell *32*, 289–300. https://doi.org/10.1091/mbc.E20-06-0398.

31. Sirajuddin, M., Farkasovsky, M., Hauer, F., Kühlmann, D., Macara, I.G., Weyand, M., Stark, H., and Wittinghofer, A. (2007). Structural insight into filament formation by mammalian septins. Nature *449*, 311–315. https://doi.org/10.1038/nature06052.

32. Maddox, A.S., Lewellyn, L., Desai, A., and Oegema, K. (2007). Anillin and the septins promote asymmetric ingression of the cytokinetic furrow. Dev. Cell *12*, 827–835. https://doi.org/10.1016/j.devcel.2007.02.018.

33. Maddox, A.S., Habermann, B., Desai, A., and Oegema, K. (2005). Distinct roles for two C. elegans anillins in the gonad and early embryo. Development *132*, 2837–2848. https://doi.org/10.1242/dev.01828.

34. Field, C.M., Coughlin, M., Doberstein, S., Marty, T., and Sullivan, W. (2005). Characterization of anillin mutants reveals essential roles in septin localization and plasma membrane integrity. Development *132*, 2849–2860.

35. Kinoshita, M., Field, C.M., Coughlin, M.L., Straight, A.F., and Mitchison, T.J. (2002). Self- and actin-templated assembly of Mammalian septins. Dev. Cell *3*, 791–802.

36. Mavrakis, M., Azou-Gros, Y., Tsai, F.C., Alvarado, J., Bertin, A., Iv, F., Kress, A., Brasselet, S., Koenderink, G.H., and Lecuit, T. (2014). Septins promote F-actin ring formation by crosslinking actin filaments into curved bundles. Nat. Cell Biol. *16*, 322–334. https://doi.org/10.1038/ncb2921.

37. Joo, E., Surka, M.C., and Trimble, W.S. (2007). Mammalian SEPT2 is required for scaffolding nonmuscle myosin II and its kinases. Dev. Cell *13*, 677–690. https://doi.org/10.1016/j.devcel.2007.09.001.

38. Kechad, A., Jananji, S., Ruella, Y., and Hickson, G.R.X. (2012). Anillin acts as a bifunctional linker coordinating midbody ring

biogenesis during cytokinesis. Curr. Biol. *22*, 197–203. https://doi.org/10.1016/j.cub.2011.11.062.

39. Hickson, G.R.X., and O'Farrell, P.H. (2008). Anillin: a pivotal organizer of the cytokinetic machinery. Biochem. Soc. Trans. *36*, 439–441. https://doi.org/10.1042/BST0360439.

40. Nguyen, T.Q., Sawa, H., Okano, H., and White, J.G. (2000). The C. elegans septin genes, unc-59 and unc-61, are required for normal postembryonic cytokineses and morphogenesis but have no essential function in embryogenesis. J. Cell Sci. *113 Pt 21*, 3825–3837.

41. Adam, J.C., Pringle, J.R., and Peifer, M. (2000). Evidence for functional differentiation among Drosophila septins in cytokinesis and cellularization. Mol. Biol. Cell *11*, 3123–3135. https://doi.org/10.1091/mbc.11.9.3123.

42. Peng, X.R., Jia, Z., Zhang, Y., Ware, J., and Trimble, W.S. (2002). The septin CDCrel-1 is dispensable for normal development and neurotransmitter release. Mol. Cell Biol. *22*, 378–387. https://doi.org/10.1128/mcb.22.1.378-387.2002.

43. Kinoshita, M. (2003). Assembly of mammalian septins. J. Biochem. *134*, 491–496. https://doi.org/10.1093/jb/mvg182.

44. O'Neill, R.S., and Clark, D.V. (2016). Partial functional diversification of Drosophila melanogaster septin genes Sep2 and Sep5. G3 *6*, 1947–1957. https://doi.org/10.1534/g3.116.028886.

45. Dragieva, Z. (2016). MSc Thesis: Caractérisation des structures de septines hautement organisées chez la drosophile et leur interaction avec le cytosquelette d'actine (Université de Montréal). http://hdl.handle.net/1866/16242.

46. Echard, A., Hickson, G.R.X., Foley, E., and O'Farrell, P.H. (2004). Terminal cytokinesis events uncovered after an RNAi screen. Curr. Biol. *14*, 1685–1693.

47. Somma, M.P., Fasulo, B., Cenci, G., Cundari, E., and Gatti, M. (2002). Molecular dissection of cytokinesis by RNA interference in Drosophila cultured cells. Mol. Biol. Cell *13*, 2448–2460.

48. Zhao, W.M., and Fang, G. (2005). Anillin is a substrate of anaphase-promoting complex/cyclosome (APC/C) that controls spatial contractility of myosin during late cytokinesis. J. Biol. Chem. *280*, 33516–33524.

49. El Amine, N., Kechad, A., Jananji, S., and Hickson, G.R.X. (2013). Opposing actions of septins and Sticky on Anillin promote the transition from contractile to midbody ring. J. Cell Biol. *203*, 487–504. https://doi.org/10.1083/jcb.201305053.

50. Longtine, M.S., DeMarini, D.J., Valencik, M.L., Al-Awar, O.S., Fares, H., De Virgilio, C., and Pringle, J.R. (1996). The septins: roles in cytokinesis and other processes. Curr. Opin. Cell Biol. *8*, 106–119. https://doi.org/10.1016/s0955-0674(96)80054-8.

51. Founounou, N., Loyer, N., and Le Borgne, R. (2013). Septins regulate the contractility of the actomyosin ring to enable adherens junction remodeling during cytokinesis of epithelial cells. Dev. Cell *24*, 242–255. https://doi.org/10.1016/j.devcel.2013.01.008.

52. Menon, M.B., and Gaestel, M. (2015). Sep(t)arate or not – how some cells take septin-independent routes through cytokinesis. J. Cell Sci. *128*, 1877–1886. https://doi.org/10.1242/jcs.164830.

53. Budnar, S., Husain, K.B., Gomez, G.A., Naghibosadat, M., Varma, A., Verma, S., Hamilton, N.A., Morris, R.G., and Yap, A.S. (2019). Anillin promotes cell contractility by cyclic resetting of RhoA residence kinetics. Dev. Cell *49*, 894–906.e12. https://doi.org/10.1016/j.devcel.2019.04.031.

54. Bertin, A., McMurray, M.A., Thai, L., Garcia, G., 3rd, Votin, V., Grob, P., Allyn, T., Thorner, J., and Nogales, E. (2010). Phosphatidylinositol-4,5-bisphosphate promotes budding yeast septin filament assembly and organization. J. Mol. Biol. *404*, 711–731. https://doi.org/10.1016/j.jmb.2010.10.002.

55. McDonald, N.A., Lind, A.L., Smith, S.E., Li, R., and Gould, K.L. (2017). Nanoscale architecture of the Schizosaccharomyces pombe contractile ring. Elife *6*, e28865. https://doi.org/10.7554/eLife.28865.

56. Schroeder, T.E. (1990). The contractile ring and furrowing in dividing cells. Ann. N. Y. Acad. Sci. *582*, 78–87. https://doi.org/10.1111/j.1749-6632.1990.tb21669.x.

57. Morris, R.G., Husain, K.B., Budnar, S., and Yap, A.S. (2020). Anillin: the first proofreading-like scaffold? Bioessays *42*, e2000055. https://doi.org/10.1002/bies.202000055.

58. D'Avino, P.P., Takeda, T., Capalbo, L., Zhang, W., Lilley, K.S., Laue, E.D., and Glover, D.M. (2008). Interaction between Anillin and RacGAP50C connects the actomyosin contractile ring with spindle microtubules at the cell division site. J. Cell Sci. *121*, 1151–1158. https://doi.org/10.1242/jcs.026716.

59. Gregory, S.L., Ebrahimi, S., Milverton, J., Jones, W.M., Bejsovec, A., and Saint, R. (2008). Cell division requires a direct link between microtubule-bound RacGAP and Anillin in the contractile ring. Curr. Biol. *18*, 25–29. https://doi.org/10.1016/j.cub.2007.11.050.

60. Frenette, P., Haines, E., Loloyan, M., Kinal, M., Pakarian, P., and Piekny, A. (2012). An anillin-Ect2 complex stabilizes central spindle microtubules at the cortex during cytokinesis. PLoS One *7*, e34888. https://doi.org/10.1371/journal.pone.0034888.

61. Magie, C.R., Pinto-Santini, D., and Parkhurst, S.M. (2002). Rho1 interacts with p120ctn and alpha-catenin, and regulates cadherin-based adherens junction components in Drosophila. Development *129*, 3771–3782.

62. Neufeld, T.P., and Rubin, G.M. (1994). The Drosophila peanut gene is required for cytokinesis and encodes a protein similar to yeast putative bud neck filament proteins. Cell *77*, 371–379.

63. Dolat, L., Hunyara, J.L., Bowen, J.R., Karasmanis, E.P., Elgawly, M., Galkin, V.E., and Spiliotis, E.T. (2014). Septins promote stress fiber-mediated maturation of focal adhesions and renal epithelial motility. J. Cell Biol. *207*, 225–235. https://doi.org/10.1083/jcb.201405050.

STAR★METHODS

KEY RESOURCES TABLE

REAGENT or RESOURCE	SOURCE	IDENTIFIER
Antibodies		
Chicken polyclonal anti-Anillin	Hickson lab El amine et al. (2019)[18]	N/A
Mouse monoclonal anti-α-tubulin (clone DM1A)	Sigma-Aldrich	Cat#CP06, RRID:AB_2617116
Rabbit Anti-Green Fluorescent Protein (GFP) Polyclonal Antibody	Molecular Probes (ThermoFisher Scientific)	Cat#A-6455, RRID:AB_221570
Mouse Anti-Drosophila Peanut Monoclonal Antibody, Unconjugated	Developmental studies hybridoma bank	Cat#4C9H4 anti-peanut, RRID:AB_528429
Mouse Anti-Drosophila Rho1 Monoclonal Antibody, Unconjugated	Developmental studies hybridoma bank	Cat# p1D9 (anti-rho1), RRID:AB_528263
Bacterial and virus strains		
Escherichia coli NEB® 5-alpha Chemically competent cells	New England Biolabs	Cat# C2987I
Escherichia coli BL21(DE3) Chemically competent cells	Sigma-Aldrich	Cat# CMC0014
Escherichia coli One Shot™ TOP10 Chemically competent cells	ThermoFisher Scientific	Cat# C404010
Chemicals, peptides, recombinant proteins		
Alexa Fluor® 647 Phalloidin antibody	Thermo Fisher Scientific	Cat#A22287, RRID:AB_2620155
Goat anti-Mouse IgG (H + L) Cross-Adsorbed Secondary Antibody, Alexa Fluor 488	Thermo Fisher Scientific	Cat#A-11001, RRID:AB_2534069
Goat anti-Mouse IgG (H + L) Cross-Adsorbed Secondary Antibody, Alexa Fluor 647	Thermo Fisher Scientific	Cat#A-21235, RRID:AB_2535804
Goat anti-Mouse IgG (H + L) Cross-Adsorbed Secondary Antibody, Alexa Fluor 546	Thermo Fisher Scientific	Cat#A-11003, RRID:AB_2534071
Aurora alpaca secondary antibody anti-chicken IgY ATTO 565 conjugated	Immune Biosolutions	Cat#Y00008-565, RRID:AB_2622026
Aurora alpaca secondary antibody anti-chicken IgY	Immune Biosolutions	Cat#Y00008-002, RRID:AB_2622024
FugeneHD transfection reagent	Promega corporation	Cat#E2311
Lipofectamine 2000	ThermoFisher Scientific	Cat#11668030
CellfectinII	ThermoFisher Scientific	Cat#10362100
Latrunculin A	Sigma-Aldrich	Cat#428021
Puromycin dihydrochloride	Sigma-Aldrich	Cat#P8833
Fluoromount-G	SouthernBiotech	Cat# 0100-01
Opti-MEM	Thermo Fisher Scientific	Cat#31985062
Fetal Bovine Serum, qualified, heat inactivated, United States	Thermo Fisher Scientific	Cat#16140071
Schneider's Drosophila medium	Thermo Fisher Scientific	Cat#21720024
Dulbecco's modified Eagle's medium DMEM, high glucose, pyruvate	Thermo Fisher Scientific	Cat#11995040
CO_2 independent medium	Thermo Fisher Scientific	Cat#18045088
Clarity Max™ Western ECL Substrate, 100 mL	Bio-Rad	Cat#1705062
Critical commercial assays		
pENTR™/D-TOPO™ Cloning Kit	Thermo Fisher Scientific	Cat#K240020

(*Continued on next page*)

Continued

REAGENT or RESOURCE	SOURCE	IDENTIFIER
T7 RiboMAX™ Express Large Scale RNA Production System	Promega corporation	Cat#P1320
Gateway LR clonase enzyme mix	Thermo Fisher Scientific	Cat#11791019
T4 DNA Ligase	Thermo Fisher Scientific	Cat#15224025
Experimental models: Cell lines		
D.melanogaster Schneider's S2 cells	University of California San Francisco	N/A
HeLa cell line	ATCC	Cat#CRM-CCL-2, RRID:CVCL_0030
S2 cells expressing Anillin-GFP and mCherry-tubulin	This paper	N/A
S2 cells expressing Anillin-RBD*-GFP and mCherry-tubulin	This paper	N/A
Oligonucleotides		
siRNA targeting sequence: pGL2 Firefly Luciferase (CGUACGCGGAAUACUUCGA)	Eurogentec	Cat#SR-CL010-005
siRNA targeting sequence: hs ANLN (CGAUGCCUCUUUGAAUAAA)	Dharmacon	N/A
Primers used for all constructs cloned, see Table S1	This paper	N/A
Recombinant DNA		
pCoPuro plasmid	Addgene	RRID:Addgene_17533
D.mel pENTR-Anillin-WT-ds resistant, pMT-Anillin-ds resistant-WG/WCh	This paper	N/A
D.mel pENTR-Anillin-RBD*-ds resistant, pMT-Anillin-RBD*-WG/WCh	This paper	N/A
D.mel pMT-Anillin-ΔC-term-WCh	Kechad et al.[38]	N/A
D.mel pENTR-Anillin-ΔN-term-ds resistant, pMT-Anillin-ΔN-term-WCh	This paper	N/A
D.mel pENTR-Anillin-ΔN-term-RBD*-ds resistant, pMT-Anillin-ΔN-term-RBD*-WCh	This paper	N/A
D.mel pENTR-Anillin-AHD-ds resistant, pMT-Anillin-AHD-WCh	This paper	N/A
D.mel pENTR-Anillin-PHD-ds resistant, pMT-Anillin-AHD-WCh	This paper	N/A
D.mel pMT-Anillin-ΔAHD-WCh	Laboratory of Gilles Hickson	N/A
D.mel pENTR-Anillin-Δ796-1050-ds resistant, pMT-Anillin-Δ796-1050-WCh	This paper	N/A
D.mel pENTR-Anillin-ΔRBD(Δ850-915)-ds resistant, pMT-Anillin-ΔRBD(Δ850-915)-WCh	This paper	N/A
D.mel pENTR-Anillin-Δ796-928-ds resistant, pMT-Anillin-Δ796-928-WCh	This paper	N/A
D.mel pENTR-Anillin-PH+54-(1051-1239)-ds resistant, pMT-Anillin-PH+54 (1051-1239)-WCh	This paper	N/A
D.mel pENTR-Anillin-PH+103-(998-1239)-ds resistant, pMT-Anillin-PH+103 (998-1239)-WCh	This paper	N/A
D.mel pENTR-Anillin-PH+206-(899-1239)-ds resistant, pMT-Anillin-PH+206 (899-1239)-WCh	This paper	N/A
D.mel pENTR-Anillin-ΔPHD-ds resistant, pMT-Anillin-ΔPHD-WCh	This paper	N/A

(*Continued on next page*)

Continued

REAGENT or RESOURCE	SOURCE	IDENTIFIER
D.mel pMT-Septin1-WG	Laboratory of Gilles Hickson	N/A
D.mel pMT-Septin2-WG and pMT-Septin2-WCh	Laboratory of Gilles Hickson	N/A
Hs pEGFP-Anillin-WT-RNAi resistant-C1	Piekny & Glotzer[10] Addgene Note this is the shorter 1087 amino acid isoform of the two isoforms of human ANLN	RRID:Addgene_68027
Hs pEGFP-Anillin-A703E-RNAi resistant-C1	Kind gift from Dr Alisa Piekny, Concordia University, Montreal, Canada. Note that this is the shorter 1087 amino acid isoform of the two isoforms of human ANLN. A703 corresponds to A740 of the longer 1124 amino acid isoform described in Sun et al.[23]	N/A
pEGFP-N1-SEPT2 (mouse)	Kind gift from Dr Elias Spiliotis, Drexel University, Philadelphia, USA	N/A
pEGFP-C3-SEPT6 (Human)	Kind gift from Dr Elias Spiliotis, Drexel University, Philadelphia, USA, Kinoshita et al.[35]	N/A
pEGFP-SEPT7 (Rat)	Kind gift from Dr Elias Spiliotis, Drexel University, Philadelphia, USA	N/A
pmCherry-N1-SEPT9 (human isoform 1)	Kind gift from Dr Elias Spiliotis, Drexel University, Philadelphia, USA Dolat et al., 2014[63]	N/A
Software and algorithms		
Volocity version 6.3	Perkin Elmer http://www.perkinelmer.com/pages/020/cellularimaging/products/volocity.xhtml	RRID:SCR_002668
GraphPad Prism 7	GraphPad http://www.graphpad.com/	RRID:SCR_002798
Adobe photoshop CS6	Adobe https://www.adobe.com/products/photoshop.html	RRID:SCR_014199
Adobe illustrator CS6	Adobe http://www.adobe.com/products/illustrator.html	RRID:SCR_010279

RESOURCE AVAILABILITY

Lead contact

Further information and requests for resources and reagents should be directed to and will be fulfilled by the lead contact, Gilles R.X. Hickson (gilles.hickson@umontreal.ca).

Materials availability

All unique reagents generated in this study are available from the lead contact.

Data and code availability

- All data reported in this paper will be shared by the lead contact upon request.
- This paper does not report original code.
- Any additional information required to reanalyze the data reported in this paper is available from the lead contact upon request.

EXPERIMENTAL MODEL AND STUDY PARTICIPANT DETAILS

Cell lines

Drosophila Schneider 2 (S2) cells (derived from a primary culture of late-stage 20-24 h old *Drosophila melanogaster* embryos obtained from university of San Francisco, California) were cultured at 25°C and ambient CO_2 in Schneider's Drosophila medium (Life Technologies) supplemented with 10% (v/v) heat-inactivated fetal bovine serum (U.S origin, Thermo Fisher Scientific) and passaged every 7 days.

Human HeLa cells (derived from cervical cancer cells taken from a human female suffering from cervical cancer) were cultured in DMEM (high glucose) supplemented with 10% (v/v) heat-inactivated fetal bovine serum (Thermo Fisher Scientific) at 37°C and 5% CO_2. Cells were cultured for up to 25 passages from thawing.

METHOD DETAILS

Molecular biology- cloning

Generation of dsRNA-resistant anillin

The *D. melanogaster* scraps isoform B (NP_724582.1) was used throughout.

A ds-RNA-resistant form of Anillin was generated by designing a 847 bp GeneArt fragment (ThermoFisher Scientific) with silent mutations in the third base in each of the last 270 codons of the Anillin ORF. The DNA fragment was synthesized to include a 'CACC' sequence at the start (5' end) to allow pENTR/D-TOPO cloning and AgeI and PmlI restriction sites for sub-cloning into the full-length cDNA sequence in pENTR.

The Anillin-RBD point mutants (Anillin-A874D, Anillin-E892K and Anillin-A874D-E892K) were generated by synthesizing a 598 bp GeneArt DNA fragment that included the designated coding mutation(s) and the optimized codons (silent mutations) exactly as the dsRNA-resistant wild-type Anillin. This DNA fragment ('insert') was then double digested with PmlI (New England Biolabs) and AscI (New England Biolabs) alongside wild-type dsRNA-resistant Anillin in pENTR plasmid ('vector'). Double digested insert and vector were gel purified and ligated (vector-to-insert ratio of 1:5) using a T4 ligase (Thermofisher Scientific) and reaction buffer for 18 h at 20°C before transforming 10 μL of ligation reaction into competent DH5a *Escherichia coli* cells (NEB 5-alpha C2987I, New England Biolabs) and growing on Luria-Bertani plates containing 100 μg/mL Kanamycin. Positive clones were verified by Sanger sequencing and recombined into the pMT-WG or pMT-WCh destination vectors (Drosophila Gateway Vector Collection; T. Murphy, Carnegie Institution for Science, Washington, DC) using LR clonase.

Anillin-ΔRBD, Anillin-Δ796-928 and Anillin-Δ796-1050 constructs were also generated by designing and synthesizing GeneArt fragments (400 bp, 300 bp and 658 bp respectively) that included a 5' 'CACC' sequence and AgeI and PmlI restriction sites. Fragments were first cloned into pENTR-D-TOPO (Invitrogen), then sub-cloned into full-length Anillin-pENTR by double restriction enzymes digest (AgeI and PmlI for Anillin-ΔRBD and Anillin-Δ796-928 and AgeI and AscI for Anillin-Δ796-1050) and ligation as described above. Resulting positive pENTR clones (verified by Sanger sequencing) were then recombined into pMT-WG and pMT-WCh destination vectors (Drosophila Gateway Vector Collection; T. Murphy, Carnegie Institution for Science, Washington, DC) using LR clonase.

Double-stranded RNA-resistant versions of Anillin-AH domain, Anillin-PH domain, PH domain extensions, Anillin-ΔN-terminus, AnillinΔN-terminus-RBD* and Anillin-ΔPH dsRNA-resistant were generated by PCR amplification of amino acids; 796-1104 (for Anillin-AHD), 1105-1239 (For Anillin-PH), 1051-1239 (for Anillin-PH+54aa), 1002-1239 (for Anillin-PH+103 aa), 899-1239 (for Anillin-PH+206aa), 796-1239 (for AnillinΔN-terminus and AnillinΔN-terminus-RBD*) and 1-1104 (for Anillin-ΔPH dsRNA-resistant) using respective forward primers that included the 5' 'CACCATG' sequence (Table S1) and a reverse primer that lacked a stop codon and using full-length ds-RNA resistant Anillin or Anillin-RBD* (in the case of Anillin-ΔN-terminus-RBD*) as a PCR template. PCR inserts were gel purified, TOPO cloned into pENTR-D-TOPO (Invitrogen) followed by Gateway recombination using LR clonase into appropriate vectors (Drosophila Gateway Vector Collection; T. Murphy, Carnegie Institution for Science, Washington, DC). Positive clones were verified by Sanger sequencing.

S2 cell transfections and RNAi

Transient DNA transfections were performed with FugeneHD (Promega Corporation) according to manufacturer's instructions using a 3:1 FugeneHD:DNA ratio with 1 μg of each plasmid DNA. Transfections were

carried out in the presence of serum. S2 cells were seeded a day prior to transfections at a density of 1.0 × 10^5 cells/mL. 1.0 μg of each plasmid DNA was diluted in 100 μL of serum-free Schneider's Drosophila medium and the appropriate volume of FugeneHD and transfection mix was incubated at room temperature for 20 min before adding drop-wise over cells in complete growth medium.

RNA interference was performed in S2 cells using long (250–800 bp) double-stranded RNAs (dsRNA). DNA templates were generated in a two-step PCR amplification process from cDNA or genomic DNA (in the case of UTR regions). The first round of PCR was performed with gene-specific primers (Table S1) that included a 5′ 8-base pair anchor sequence (GGGCGGGT). In the second PCR, a universal T7 primer containing the anchor sequence (5′-TAATACGACTCACTATAGGGAGACCACGGGCGGGT-3′) was used to generate gene-specific PCR templates that included the T7 promoter sequence at the 5′ end. Ds-RNAs were subsequently generated by *in vitro* transcription (T7 RiboMAX Express, Promega Corporation) overnight at 37°C. After RQ1 DNase digestion of the template cDNA, the resulting RNAs were then precipitated in ethanol, resuspended in nuclease-free water, denatured at 95°C, and slowly cooled to room temperature to allow the RNA to anneal and form dsRNAs, which were then verified by agarose gel electrophoresis and quantified.

For RNAi experiments, S2 cells were plated at a density of 1.2 × 10^5 cells/mL in a 96-well plate and treated with 1 μg/mL of dsRNA for 3–7 days (indicated in the figure legends). In the case of 7 days of RNAi, two rounds of dsRNA treatment were performed-cells were split 1:1 into fresh complete medium 3 days after the first dsRNA treatment followed by the addition of 1 μg/mL of fresh dsRNA and incubation for a further 4 days. RNAi experiments in stable cell lines were carried out 2 weeks after the 7-day selection period, and in the case of transient transfections, dsRNA incubation was initiated 1 day after transfection. Expression of fluorescent protein fusions under the control of the metallothionein promoter (pMT plasmids) was induced by the addition of a final concentration of 0.5 mM copper sulfate 24 h prior to imaging and 30 min after dsRNA treatment in the case of rescue experiments. Live imaging was carried out 3 days after RNAi for *anillin* RNAi (dsRNA1), 4 days for *spaghetti squash* (myosin regulatory light chain) RNAi and 7 days for *pnut*, *septin2* and *anillin* 3′UTR RNAi. dsRNAs against LacI was included in every experiment as a negative control. For Latrunculin A (LatA) experiments, LatA (Calbiochem/Millipore Sigma) dissolved in DMSO was diluted in growth medium and gently pipetted onto the cells to a final concentration of 1 μg/mL, 10 min prior to the start of image acquisition.

HeLa cells transfection and RNAi

RNA interference in HeLa cells was performed using Lipofectamine 2000 (Thermo Fisher Scientific) and suitable siRNA oligos according to manufacturer's instructions. pGL2 Firefly Luciferase (CGUACGC GGAAUACUUCGA) (Eurogentec) was used as a negative control. ANLN was targeted with 50 nM of a double-stranded small interfering RNA (CGAUGCCUCUUUGAAUAAA, Dharmacon, Piekny, A & Glotzer, M., 2008[10]). HeLa cells were plated in glass-bottomed 8-well chamber slides (LabTek II) at a density of 2.5 × 10^5 cell/mL (to about 80% confluency) and immediately co-transfected whilst in suspension, with siRNA and DNA using Lipofectamine 2000, which was used at 8-fold less than manufacturer's recommendations. First, Lipofectamine 2000 was diluted in OPTI-MEM and incubated at room temperature for 5 min. Meanwhile, 50 nM siRNA and 0.75 μg of DNA were diluted in OPTI-MEM and then the siRNA+DNA+OPTI-MEM mix was added to the Lipofectamine 2000 + OPTI-MEM mix and incubated for a further 20 min before adding drop-wise over the cells and incubating at 37°C/5% CO_2 for 24 h. The medium over cells was replaced with CO_2-independent medium (Thermo Fisher Scientific) 1 h prior to live imaging.

Live cell microscopy

S2 cells were plated into fresh Schneider's medium in an 8-well chamber slide (Lab-Tek II) the day before imaging and time-lapse imaging of S2 cells was performed using a spinning-disc confocal system (UltraVIEW Vox; PerkinElmer) using a scanning unit (CSU-X1; Yokogawa Corporation of America) and a charged-couple device camera (ORCA-R2; Hamamatsu Photonics) fitted to an inverted microscope (DMI6000 B; Leica) equipped with a motorized piezoelectric stage (Applied Scientific Instrumentation). Image acquisition was controlled using Volocity version 6.3 (PerkinElmer) and was performed in emission discrimination mode. Low resolution time-lapse imaging was performed using a Plan Apochromat 40× 0.85 NA air objective with camera binning set to ×2 and 10 μm Z stacks were acquired with an optical spacing of 1 μm at 5 min intervals overnight. High-resolution imaging was performed using a Plan Apochromat 63× oil immersion objectives, NA 1.4, with camera binning set to 2 × 2 and Z stacks were acquired

with an optical spacing of 0.5 μm at 2–3 min intervals, unless otherwise stated in the figure legends. HeLa cells were imaged on the same system, but using a stage-top imaging chamber to maintain the cells and objectives at 37°C.

Immunofluorescence microscopy

S2 cells were fixed in 4% paraformaldehyde diluted in 1x Phosphate buffered saline (PBS) for 15 min at room temperature, followed by a wash in 1xPBS and permeabilization in PBS containing 0.1% (v/v) Triton X-100 (PTX) for 5 min. Cells were then blocked for 1 h in blocking solution, PBS containing 0.1% Triton X-100 and 5% (v/v) Normal goat serum (NGS). Cells were then washed three times in PTX before incubating with primary antibodies diluted in blocking solution overnight at 4°C using the following dilutions: chicken anti-Anillin (*Drosophila*) polyclonal (1 in 500) (Hickson lab[18]), mouse anti-Peanut (1 in 500) (monoclonal 4C9H4 supernatant, Developmental Studies Hybridoma Bank), mouse anti-Rho1 (monoclonal p1D9 supernatant, Developmental Studies Hybridoma Bank) and mouse anti-α-tubulin (1 in 1000) (monoclonal DM1A clone, Sigma-Aldrich). Cells were washed three times in PTX before incubating in Alexa 488- or Alexa 546- (used at 1:500) or Alexa 657-conjugated secondary antibodies (used at 1:200) (refer to KRT for details) and Hoechst 33242 diluted in blocking solution for 1 h in the dark at room temperature. Cells were washed again three times in PTX and a final wash in PBS before mounting in 100 μL/well of Fluoromount-G (Southern Biotech). Images were acquired using the UltraVIEW Vox system described in the preceding section using a Plan Apochromat 63 ×1.4 NA oil immersion objective in emission discrimination mode with a Z optical slicing of 0.5 μm and without camera binning.

Image analysis (contractile ring closure and ratio of cortical versus cytoplasmic recruitment)

Quantification of 4D datasets (x,y,z and time) was performed using Volocity 6.3 quantitation. Contractile ring closure measurements were performed using the line tool. The furrow was visualized by GFP-tagged Anillin-WT or Anillin-ΔPH or Anillin-RBD* and its diameter was measured starting at anaphase onset (time = 0), by drawing a line across the nascent contractile ring (cortex-to-cortex) starting at anaphase onset (time = 0). It was ensured that the line drawn was perpendicular to the central spindle (as visualized by mCh-tubulin) and passing through the center of the spindle. Furrow diameter was measured for each timepoint and ring closure was defined to occur at the first timepoint at which furrow diameter was 1 μm (or close to 1 μm) and was consistently 1 μm or less at subsequent time points.

The cortical enrichment of GFP/mCherry-tagged proteins was calculated by dividing the mean of the peak background-corrected GFP/mCherry fluorescence intensities at the cortex by the mean of the background-corrected adjacent sub-cortical (cytoplasmic) intensities. Fluorescence intensity values were obtained from line profiles by drawing a line across the cell equator at 2–3 min after anaphase onset. The lines were extended beyond the cell on either side of the furrow into the dark space between cells, to determine the average background fluorescence intensity for background correction. Images were processed for publication using Photoshop CS6 (Adobe) and assembled as figures using Illustrator CS6 (Adobe). Video files were exported from Volocity as QuickTime videos (Apple).

Recombinant protein expression

GST-tagged proteins were expressed in BL21 *E. coli* cells. A 3 mL culture of *E. coli* cells transformed with either the construct of interest or a GST only control, was grown overnight in LB with 50 μL/mL of Ampicillin at 37°C with shaking at 220 rpm. The following day, these starter cultures were used to inoculate 300 mL of fresh LB + Ampicillin and cells were grown at 37°C with shaking until the cultures reached an optical density (OD) reading at 600 nm (A_{600nm}) of 0.6. Recombinant protein expression was then induced by addition of 0.1 mM isopropyl β-Δ-1-thiogalactopyranoside and further incubation at 37°C for 4 h with shaking. Bacterial cells were harvested by centrifugation at 6000 × *g* at 4°C followed by resuspension of the pellet in lysis buffer (20 mM HEPES, pH 7.4, 0.2 M NaCl, 1 mM EDTA, 5 mM MgCl2, 0.1% Triton X-100, 1 mM dithiothreitol, 1 mg/mL lysozyme, 0.2 mg/mL Pefabloc), supplemented with complete protease inhibitors (Roche), and lysed at 4°C on ice for 2 h (with intermittent resuspension). Bacterial lysates were then sonicated on ice for 5–10 min using a cycle alternating between 30 s of pulse and 30 s of rest at 50% amplitude. Sonicated lysate was cleared by centrifugation at 12,000 × *g* for 20 minat 4°C and then applied to prewashed glutathione Sepharose beads (GE healthcare) overnight at 4°C with rotation. GST-tagged proteins bound to beads were separated from the unbound proteins by centrifugation at 5000 rpm at 4°C for 15 min followed by three washes in HMNT lysis buffer (20 mM HEPES, pH 7.4, 10 mM $MgCl_2$, 0.1 M NaCl, 0.5% Triton X-100).

Washed GST-protein bounds to beads were immediately incubated with pre-cleared whole cell lysate containing prey protein in HMNT buffer, at 4°C with constant rotation overnight.

Whole cell extract preparation

Wild-type S2 cells were cultured in T75 culture flasks for 7 days and induced with 0.5 mM Copper sulfate (final concentration) 72 h before harvesting by centrifugation at 1100 rpm for 5 min. Cell pellets were washed twice in ice-cold PBS prior to lysis in 1 mL of HMNT buffer per T75 flask (20 mM HEPES, pH 7.4M 10 mM $MgCl_2$, 0.1M NaCl, 1% Triton X-100 supplemented with 1 mini tablet of EDTA-free protease inhibitor cocktail, Thermo Fisher Scientific) for 1–2 h on ice, with intermittent vortexing. Extracts were clarified by centrifugation at 13,200 rpm for 20 min at 4°C in a microfuge and either incubated immediately with protein on beads at 4°C or flash frozen in liquid nitrogen for future use. For protein knockdown experiments, wild-type S2 cells were grown in eight wells of a 96-well plate per condition and treated with relevant dsRNA for 3–7 days before pooling the contents of the eight wells and harvesting by centrifugation at 1100 rpm for 5 min, washed twice in PBS and extracted in HMNT buffer (100 μL for 8 wells) as above. The concentration of protein on beads and whole cell extracts were measured using the BCA assay (Pierce BCA protein assay kit; Thermo Fisher Scientific).

GST pull down assay

S2 cell extract (500 μL/pull down at 2.0 mg/mL) was cleared by ultra-centrifugation at 55,000 rpm for 20 minat 4°C and incubated with glutathione Sepharose beads containing GST-tagged bait protein (150 μg/pull down) or GST alone overnight at 4°C on a rotating platform (total volume of pull down reaction is 1 mL). After binding, beads were centrifuged at 5000 rpm for 5 min at 4°C to collect the unbound fraction which was then denatured in an appropriate volume of 6xSDS sample buffer (for a final volume of 1 mL), by boiling at 95°C for 5 min. Beads were then washed 3 times in cold HMNT buffer and the bound fraction was eluted in a volume of 2x SDS sample buffer (for a final volume of 1 mL), by boiling at 95°C for 5 min and centrifugation at 13, 200 rpm for 5 min.

Immunoblot

Protein samples were subjected to SDS polyacrylamide gel electrophoresis (8–10% polyacrylamide). For assessing the efficiency of RNAi-mediated depletion, equal dilutions of protein from control or gene-specific dsRNA-treated samples were loaded whilst for GST pull down assays, equivalent percentages (v/v of the initial pull down reaction) of bound and unbound fractions were loaded. Following SDS-PAGE separation, proteins were transferred onto Amersham Protran nitrocellulose membrane (0.45 μm pore size) at 4°C using constant current (300 mA) for 2.5–3 h. Membranes were stained with Ponceau S, digitally scanned, then blocked with 5% milk in PBS containing 0.15% Tween20 (PBS-T; blocking solution) for 1 h at room temperature. Where appropriate, membranes were cut at the relevant molecular weight marker and incubated in blocking solution containing primary antibody overnight at 4°C on a rocking platform [Chicken anti-Anillin polyclonal used 1:2000, mouse anti-tubulin (clone DM1A, Sigma-Aldrich) used 1:2500, concentrated mouse anti-Peanut (clone 4C4H9, Developmental Studies Hybridoma Bank)]. Membranes were washed 3 times in PBS-T and incubated with either horseradish peroxidase–conjugated donkey anti-rabbit, anti-mouse secondary antibody (1:4000; GE Healthcare), or alpaca anti-chicken (1:4000; Immune Biosolutions) in blocking solution for 1 h at room temperature on a rocking platform, followed by washing in PBS-T and signal development with Clarity Western ECL substrate (Bio-Rad) and visualization on a ChemiDoc MP imaging system (Bio-Rad).

QUANTIFICATION AND STATISTICAL ANALYSIS

Statistical analysis

At least three independent repeats were carried out for each experiment (unless otherwise stated in the figure legends). Statistical analyses were conducted comparing independent experiments with use of GraphPad Prism 7 software (GraphPad Software). Gaussian distribution of data was assessed using the D'Agostino-Pearson test. Means were compared using an unpaired Student's *t* test to analyze data with a normal distribution. The two-way ANOVA was performed using Sidak's multiple comparisons test. The total number of cells quantified (*N* value), p values, and significance levels are indicated in the respective Figure legends.